Master's thesis

NTNU
Norwegian University of Science and Technology
Faculty of Information Technology and Electrical Engineering
Department of Electric Power Engineering

Oda Skeie

A Control Strategy for Seamless Interconnection of Microgrids in a Multigrid Configuration

Master's thesis in Energy and Environmental Engineering
Supervisor: Olav Bjarte Fosso
Co-supervisor: Dr. Merkebu Zenebe Degefa, Dr. Salvatore D'Arco
June 2021

NTNU
Kunnskap for en bedre verden

Oda Skeie

A Control Strategy for Seamless Interconnection of Microgrids in a Multigrid Configuration

Master's thesis in Energy and Environmental Engineering
Supervisor: Olav Bjarte Fosso
Co-supervisor: Dr. Merkebu Zenebe Degefa, Dr. Salvatore D'Arco
June 2021

Norwegian University of Science and Technology
Faculty of Information Technology and Electrical Engineering
Department of Electric Power Engineering

NTNU

Kunnskap for en bedre verden

Abstract

The integration of renewable energy sources in the power grid results in more distributed power generation relative to the traditional grid structure. The new grid characteristics have caused the concept of microgrids to attract more attention. A central advantage of microgrids is that they can be operated in both stand-alone and grid-connected mode. Since they are able to operate in stand-alone mode, implementation of microgrids is seen as a good approach to enforce electrification in rural areas.

To enhance the reliability and flexibility of the microgrids in these areas, where connecting to the utility grid might not be possible, interconnecting several microgrids to form a multigrid configuration is advantageous. Interconnecting microgrids arise several technical difficulties, and a vital challenge is to provide a seamless transition from stand-alone to interconnected operation. Upon interconnection, the microgrids need to be synchronized to avoid high inrush current transients at the interconnection moment.

The purpose of this thesis is to propose a synchronization technique to enable a seamless transition from stand-alone to interconnected operation with two microgrids. The proposed technique centers around synchronizing frequency and phase angle of one of the microgrids to match the other microgrid. The synchronization control commands are obtained from grid voltage measurements of both grids. The voltage measurements are used to calculate the phase angle and frequency deviations between the two grids. The deviations are passed through parallel PI controllers and added together to form a frequency offset signal, which is passed on to the synchronizing microgrid. The frequency offset from the synchronization control loops is added to the speed reference of the synchronous generator unit in the microgrid.

The proposed synchronization technique is tested in simulations. The simulation model consists of two simple microgrid models, both consisting of a synchronous generator, a converter-based generating unit and a local load. The two modeled microgrids are connected through a switch. The synchronization control loops are located at the switch, using grid voltage measurements at each side of the switch.

A simulation was conducted on a reference scenario. This showed that the synchronization loops successfully eliminated the deviations in phase angle and frequency between the two microgrids, and thus prevented high inrush currents at the interconnection moment. To test the robustness of the proposed synchronization technique, several simulations were conducted with different grid conditions. The simulations showed that the synchronization process requires a longer time interval for larger frequency deviations, larger power production from the converter-unit, larger system inertia and variations in load during the synchronization process. Some grid conditions challenged the proposed control strategy and resulted in more oscillations in the phase angle and frequency deviation response. However, the simulations show that the proposed synchronization strategy effectively eliminate deviations in phase angle and frequency between the two microgrids.

Sammendrag

Mikronett er et konsept som har fått økt oppmerksomhet i takt med økt distribuert kraftproduksjon i kraftnettet. Mye av grunnen til økningen i distribuert produksjon er at det integreres mer fornybare energikilder. En sentral fordel med mikronett er at de kan driftes både på egenhånd og koblet til det sentrale kraftnettet. At de kan driftes uten tilkobling til kraftnettet gjør at integreringen av mikronett blir sett på som en god måte å gjennomføre elektrifiseringen av rurale strøk.

I rurale strøk er det ikke nødvendigvis mulig å koble mikronett opp mot det sentrale kraftnettet. For å øke påliteligheten i disse rurale mikronettene er det i stedet fordelaktig å sammenkoble flere mikronett. Ved å koble sammen mikronett oppstår det flere tekniske utfordringer. En sentral utfordring er knyttet til å sikre en sømløs sammenkobling mellom mikronettene. Før mikronett kan sammenkobles må de synkroniseres slik at de ikke blir utsatt for høye innkoblingsstrømmer ved koblingstidspunktet.

I denne oppgaven er det utarbeidet en kontrollstrategi for å synkronisere to mikronett, og gi en sømløs overgang fra øydrift til sammenkoblet drift. Den foreslåtte kontrollstrategien har som mål å synkronisere frekvensen og fasevinkelen til et av mikronettene slik at de sammenfaller med det andre mikronettet. Fra spenningsmålinger i de to mikronettene regnes de individuelle frekvensene og fasevinklene ut. Fra disse utregningene sendes frekvens- og fasevinkelforskjellene gjennom PI-kontrollere før de legges sammen. Resultatet er et kontrollsignal som sendes til et av mikronettene. Dette kontrollsignalet blir så brukt til å justere referansen for vinkelfrekvens i mikronettets synkrongenerator.

Den foreslåtte kontrollstrategien er testet gjennom flere simuleringer. Simuleringsmodellen består av to enkle mikronettmodeller, begge bestående av en synkrongenerator og en omformerbasert generator som forsørger en lokal last. De to modellerte mikronettene er koblet sammen med en bryter. Kontrolløkken ansvarlig for synkroniseringen av mikronettene er plassert ved denne bryteren.

Det ble utformet et referansescenario for modellen som ble testet i en simulering. Resultatet viste at den foreslåtte kontrolløkken effektivt klarte å eliminere forskjellene i vinkelfase og frekvens mellom de to mikronettene. Kontrolløkken klarte dermed å forhindre at det oppstod store innkoblingsstrømmer på koblingstidspunktet. For å teste hvor robust den foreslåtte synkroniseringsstrategien er ble flere simuleringer gjennomført under ulike forhold i mikronettet. Disse simuleringene viste at synkroniseringsprosessen krevde lengre tid dersom frekvensforskjellen var større, mer av strømproduksjonen kom fra omformerenheten, treghetskonstanten hos synkronmaskinen var større eller om det oppstod en lastvariasjon under synkroniseringen. Under noen tilfeller bød forholdene i mikronettet på utfordringer for den foreslåtte strategien i form av mer svingninger i systemresponsen. Det generelle inntrykket er derimot at den foreslåtte synkroniseringsstrategien effektivt synkroniserer de to mikronettene.

Preface

This thesis concludes my final semester as a M.Sc. student at the Department of Electric Power Engineering at the Norwegian University of Science and Technology. The thesis is a continuation of the specialization project completed in the fall of 2020, titled 'Microgrid Control Strategies and Synchronization Methods Upon Connection with External Grid'.

The completion of this master thesis would not have been possible without the help of several contributors. Firstly, I would like to thank my supervisor Olav Bjarte Fosso for continuous support and guidance. Thank you for providing me with the opportunity to work on this interesting topic, it has been both challenging and rewarding.

I also wish to express my gratitude towards Dr. Merkebu Zenebe Degefa and Dr. Salvatore D'Arco at SINTEF Energy who contributed with valuable guidance throughout my thesis work. Dr. Salvatore D'Arco was available whenever technical help or assistance was needed to move foreword in my work.

I gratefully acknowledge the "MultiGrid" (NO. Ref. 285180, IN. Ref. INT/NOR/RCN/P-04/2019) project consortium for supporting the work. I would also like to thank the Research Council of Norway and Department of Science and Technology in India.

I want to thank my parents, for their support, encouragement and offer to proofread my work. Lastly, I would like to give a special thanks to my friends for keeping me motivated throughout this past year.

Trondheim June 10th, 2021

Oda Skeie

Table of Contents

List of Figures

List of Tables

List of Abbreviations

AC	Alternating Current
DC	Direct Current
HVDC	High Voltage Direct Current
PI	Proportional Integral
PLL	Phase Locked Loop
pu	Per Unit
PV	Photo-Voltaic
PWM	Pulse Width Modulation
VCO	Voltage Controlled Oscillator

1 Introduction

The integration of renewable energy sources in the power grid results in more distributed power generation relative to the traditional grid structure. With increased generation from renewable energy sources, the power system becomes more complex. The reason is the increased amount of power electronics interfacing the renewable energy generation to the grid, and the bidirectional power flow due to the fact that generation will be more decentralized than in the traditional power system structure. The changing characteristics of the power system have resulted in new technological development to achieve smarter power grid management.

Microgrids are gaining a lot of attention as a robust and cost-effective alternative to the traditional approach of centralized grids [1]. The implementation of microgrids will increase the reliability and power quality in the power system. In addition, microgrids allows efficient integration of renewable energy sources [2]. With these advantages, microgrids are seen as a solution to meet the increasing energy demand and be part of the solution to avoid energy shortage. Microgrids have also the great advantage that they are able to operate in both islanded and grid connected mode. Thus, they are seen as a suitable approach to enforce electrification of rural areas where the geographical location or the economic situation of a community prevents connection to the utility grid [3]. Microgrids may be an economically advantageous alternative to extensive expansions of the utility grid, and will contribute to increase viable access to electricity in remote regions.

Traditionally, microgrids can operate in both islanded and grid-connected mode. However, with microgrids situated in rural areas, connection to the utility grid might be difficult. The interconnection of several neighboring microgrids to a multigrid configuration can thus be an advantageous alternative. It will result in a more reliable and flexible system, in contrast to systems where microgrids operate solely in islanded mode. However, the interconnection of microgrids, and the possible connection of the multigrid configuration to a utility grid, will present several technical difficulties. The general consensus is that the control design is essential to provide reliable operation of the microgrids.

In order to enable interconnection of microgrids, a smooth transition from frequency control to frequency follower mode must be provided when switching from islanded to grid connected mode. In addition, the microgrids need to synchronize before interconnecting, this to avoid high inrush currents and transients in the system. In a multigrid configuration, the challenge of interconnecting weak grids arises as it complicates the synchronization process. Decisions regarding which microgrid should synchronize to the other, or if both should synchronize toward a common reference operating point, needs to be addressed.

This thesis is connected to SINTEF's project "MultiGrid", in collaboration with the Indian Institute of Technology Bhubaneswar. Within the next 5 years, the Indian government is planning to built 10000 microgrids to support the electrification of rural India. The goal of the project is to draft synchronization strategies and develop interconnection protocols for largely spread microgrids.

The purpose of this thesis is to propose a synchronization control strategy that provides a seamless interconnection between stand-alone microgrids. The synchronization strategy needs to enable a transition from stand-alone to interconnected operation without the risk of high inrush current transients. To ensure this, frequency, voltage and phase angle deviations between the microgrids need to be diminished within allowable limits. The

proposed synchronization technique will be tested through simulations to verify that the requirements for transitioning from stand-alone to interconnected operation are fulfilled.

The thesis is organized with the following sections:

- *Section 2* provides an overview of the microgrid concept. This section, apart from the last subsection, is a summary of some of topics considered in the literature study performed in the specialization project.
- *Section 3 and 4* provide background knowledge on the generating units which are included in the multigrid model used in the thesis.
- *Section 5* presents the proposed synchronization strategy and the methods used to obtain the control loop parameters.
- *Section 6* presents the simulation model of the multigrid is presented, along with the parameter values of each component.
- *Section 7* presents the results from the simulations performed in this thesis work.
- *Section 8* provides an overall discussion on the thesis work.
- *Section 9* draws the final conclusion made from the obtained simulation results.
- *Section 10* lists some proposals as to what can be addressed in further work on this topic.

2 Microgrids

This section is included to provide an overview on the microgrid concept, and includes relevant topics related to the interconnection of several microgrids. This section, apart from the last subsection, is a summary of some of the topics addressed in the specialization project.

The concept of microgrids is gaining a lot of attention as an efficient way to integrate the world's increasing amount of renewable power generation, and is expected to supply a significant amount of power into the future power grid. The microgrid concept is not strictly defined, but a much used definition of microgrids is defined by the US Department of Energy [4]. This states that a microgrid is defined as;

> "a group of interconnected loads and distributed energy resources within clearly defined electrical boundaries that acts as a single controllable entity with respect to the grid. A microgrid can connect and disconnect from the grid to enable it to operate in both grid-connected or island-mode."

There are many advantages of microgrids that are described in relevant literature. The possibility of operating in both islanded and grid-connected mode increases the reliability of the system as it can switch to islanded operation in case of a fault. Similarly, it can switch back to grid-connected mode to receive power support and increase power quality when it is overloaded [5]. Power losses will be reduced as the power generation is distributed, and thus it is closer to the loads. In addition, waste heat from the distributed

generating units can be utilized in combined heat and power systems that increase the efficiency of the generators. Microgrids are also able to support plug-and-play operation where loads and generating units can be connected and disconnected from the microgrid. This means that the microgrids can be expanded and scaled down without extensive re-engineering. Another advantage related to islanded operation is that microgrids can be built in rural areas to provide cost saving electricity access to remote areas [6].

The microgrid concept, however, does present some challenges. As microgrids can include a wide range of distributed energy sources, both power electronic interfaced generation and synchronous generation, the microgrid will have higher complexity than traditional grids [7]. Power generation from renewable energy sources, such as solar and wind, is intermittent and unreliable due to the dependability on variations in weather. In addition, loads with unpredictable variations in demand complicate the task of maintaining the balance between generation and demand [2]. With the presence if disturbances, such as unpredictable variation in load and production, the system will be more subject to complex transients which may lead to the appearance of unbalanced voltages, flashovers, frequency shifts and overvoltages [8]. An important challenge with microgrids is the implementation of protection of the lines and equipment. Microgrids support bidirectional current flow, contrary to traditional grids without distributed generation. In addition, microgrids include more flexible and converter-based generation, which makes it a challenge to ensure high enough short circuit currents to activate current relays [9]. Finally, the transition between islanded and grid-connected operation, in AC microgrids, provide challenges. The microgrids need to be synchronized before they connect to another grid to avoid large inrush currents transients.

2.1 Microgrid control

Microgrids may consist of different generation units, such as renewable solar and wind power, and synchronous generation such as hydro and gas. This makes the microgrid configuration intricate due to many complex components. To ensure stable operation at all times the microgrid needs to have a proper control system. The control system needs to account for both islanded and grid-connected operation, and address multiple issues. The control system must regulate voltage and frequency, control power sharing between units, handle voltage sags and imbalances, comply with plug-n-play capabilities, optimize operating costs and synchronize the microgrid upon transition to grid-connected mode [10].

The most widespread architecture for microgrid control systems has a hierarchical structure. The many tasks to be executed by the control system have different time spans and significance. It is thus beneficial to organize the tasks into different control levels [10]–[12]. The hierarchical structure is usually divided into the three levels; primary, secondary and tertiary. The main objective of the primary control level is to locally ensure responsible operation of each decentralized generation unit or energy storage system. This includes control of local power, voltage and current while following set-points given by upper level controllers. The primary control level also deals with power sharing among the generating units of the microgrid. The secondary control level deals with management of the total microgrid system, such as power quality, distributed generation unit coordination and synchronization with the utility grid or other microgrids. The tertiary control level deals with the overall issues related to optimization, power flow exchange with external grids and the overall system regulations and security.

The primary control level has local focus and is designed with decentralized control methods. All control commands are based on measurements at the unit output terminal. The primary control also needs to take into account if the microgrid operates in islanded or grid-connected mode. In islanded control some units need to operate in grid-forming mode to regulate the microgrid voltages and frequency. In grid-connected mode, the units operate in grid-following mode where the voltages and frequency set points are established by the connecting utility grid. Frequently used primary level control techniques of converter units are active and reactive power (P/Q) control, voltage and frequency (V/f) control, and droop control [13]–[15].

The upper levels and the task of power sharing in the primary level, however, deals more with the overall state and condition of the microgrid. For this reason, the control techniques in microgrid control systems usually have a centralized approach. A centralized approach could be to have a central microgrid controller which sends control commands to the microgrid units through communication links. Another could be to have a master-slave configuration where one unit is appointed the master unit with the overall responsibility of the system operation. The other units in the system will then operate as slaves which respond to changes at the master unit. The microgrid could, however, also be designed with a decentralized or distributed control approach. In decentralized control approaches, such as peer-to-peer technique, there is no communication among the units. The control in these methods are based on local measurements at the generating units. The distributed control approach combines the benefits from both the centralized and decentralized control approach. The most investigated distributed control approach is the multi agent system.

2.2 Synchronization and interconnection

In the case of AC microgrids, the microgrids need to be synchronized in frequency, phase angle and voltage magnitude before they can be interconnected. This means that the deviations in these values between the grids need to be within the allowable limits. If the interconnecting grids are not synchronized within these allowable limits upon connection, large inrush currents may occur which can cause damage to the equipment and loads. This requires the microgrids to undergo a synchronization process before they are interconnected [16]. In literature, much research is completed on the topic of synchronizing a microgrid to the utility grid. However, there is little research to find on the topic of synchronizing microgrids to be interconnected with each other.

One of the main advantages of the microgrids is that they can operate in islanded mode. The frequency and voltages in islanded microgrids are determined by the balance between production and demand within the microgrid. Microgrids are well suited for integration of renewable energy sources, such as wind and solar power generation. Thus, the frequency and voltages of islanded microgrids will vary based on the intermittent production from these generation units. Consequently, microgrids will not necessarily follow fixed frequency and voltages during islanded operation. However, as microgrids supply loads, the voltage magnitude will be kept close to 1 in per unit (pu) value to supply the loads with required power quality. The power balance of the islanded microgrids will contribute to the fact that when two islanded microgrids are to be connected they might deviate in operating point, especially in frequency and phase angle.

For microgrids with only converter units, the process of synchronization is not a problem. The converters may instantly change their frequency and phase angle with a simple phase-

locked loop. The discontinuity in the output signal will not harm any equipment. However, with rotating generating units or loads present in the microgrid, it is not possible to abruptly change phase angle and frequency. The reason is the presence of inertia. Abrupt changes in frequency may cause instability as the speed of the rotating components will increase or decrease substantially. Therefore, synchronization of microgrids containing rotating generation units or loads require the synchronization process to take place over a longer time period.

Another aspect that needs to be addressed concerning synchronization of microgrids, is to establish which reference frequency, phase angles and voltage magnitudes the microgrids are to be synchronized to. Upon the connection of two microgrids, one of the microgrids could synchronize to the other, or both microgrids could synchronize towards a common reference point in the middle.

When operating a microgrid in islanded mode, at least one of the units in the grid needs to act as a grid-forming unit, and regulate the set points of frequency and voltage in the grid to keep them at rated values. In the cases where microgrids connect with the utility grid, the grid-forming unit(s) of the microgrids switch to operate in grid-following mode. When connecting two microgrids, both microgrids cannot switch to operate all their units in grid-following mode. One of the microgrids needs to continue with units operating in grid-forming mode to ensure continuous and stable operation.

2.3 Weak grid characteristics

Although it is an advantage of microgrids to be suited for renewable energy source integration, the increased penetration of converter-based generation present some additional stability challenges. As the converter-based generation increase, the share of production from rotating generation units directly connected to the microgrid will decrease [17]. A consequence of this is that the amount of inertia in the microgrid decreases. To have inertia available in the system is important for the grid stability. In the occurrence of a contingency that result in the frequency deviating from nominal value, inertial and primary frequency response in rotating machines will prevent the system from frequency and phase angle instability issues.

A second challenge with decreasing amount of synchronous generators in the system is related to short-circuit level. The short-circuit level is a measure of the amount of available short circuit current which flows through a system during a fault [18]. A stronger system, with high short circuit level, will be able to quickly enable protection relays to trip circuit breakers and prevent widespread damage.

Synchronous generators have the ability to maintain their output voltage, if a fault occurs in a system, by regulating the excitation current of the machine. In addition, since the rotating synchronous generators are directly connected to the grid, their internal reactance affect the equivalent impedance of the grid seen from the fault site. With less synchronous generators and more non-synchronous units in the microgrid, the impedance seen from the fault site increases and accordingly reduces the short circuit level. The non-synchronous units are connected to the grid through converters instead of being directly connected and will thus not contribute to the short circuit current.

Grid strength is also related to grid impedance. High impedance in the system gives weak grid characteristics. High penetration of converter-based generation and integration of renewable energy sources result in higher grid impedance [19]. Since these components

are prevalent in microgrid structures, microgrids tend to have higher grid impedance than traditional AC distribution grids.

Thus, the integration of converter-based generation in microgrid configurations results in lower levels of inertia, lower short-circuit level and higher grid impedance than traditional grids. Hence, microgrids will often have weak grid characteristics and have higher risks of voltage instability issues.

3 Voltage Source Converter

Power electronics are becoming more and more present in power grid systems. One such power electronic component is the voltage source converter. The voltage source converter is much used in HVDC transmission, connecting the DC system to the AC systems. It is also used to connect AC areas with different operational values such as different nominal frequency. The voltage source converter also plays an increasingly important role in the integration of renewable energy sources to the grid.

A voltage source converter is used to convert between DC and AC voltages. The converter provides output that coincide with the voltage magnitudes and frequency of the grid. In addition to convert between AC and DC voltages, the voltage source converter can also contribute with services to the grid, such as enhance efficiency and reliability, and provide filtering and power compensation in the power system.

The 2-level voltage source converter is composed of completely controllable and unidirectional switches, each connected in parallel with a diode. The switches are arranged in three legs, one for each phase, where each leg consist of an upper and a lower valve of switches. The general architecture of the voltage source converter is shown in Figure 1. In high power, high voltage system, a valve can consist of a series of switches to be able to handle the voltage and current requirements. The switches are controlled by gate signals to control the output voltages of the converter where only one of the valves in each leg is conducing current at the time. An active filter is applied at the output of the converter to provide a smoother sinusoidal waveform.

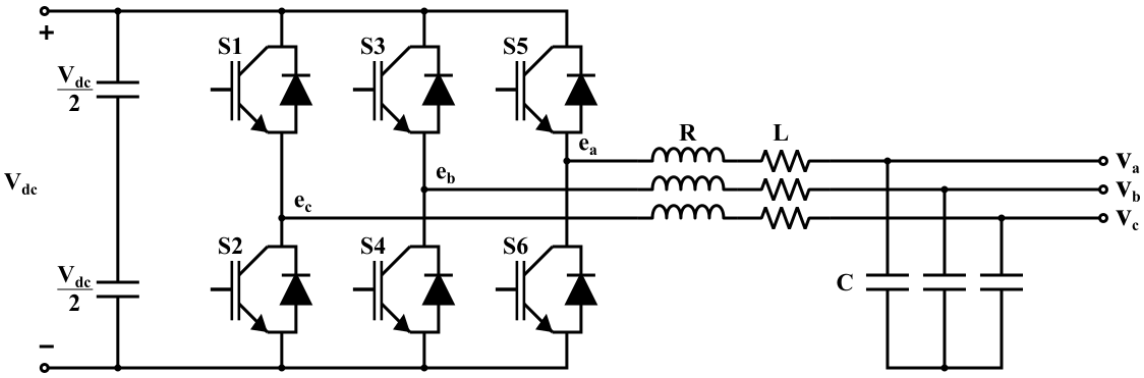

Figure 1: General architecture of a voltage source converter.

3.1 Average model

Modeling of voltage source converters can be achieved either by using the switching model or the averaged model of a converter [13]. In the switching model the gate signals directly command the status of the switches. The gate signals will turn on and off to lead the current either through the upper valve or the lower valve of a leg, resulting in an output voltage switching between the negative and positive value of the DC side voltage, $-V_{dc}$ and V_{dc}.

The switching model provides accurate description of the steady-state and dynamic behavior of the converter, including high frequency components. However, the time step is required to be sufficiently small depending on the switching frequency of the device. Additionally, the relationship between the modulation signal and the output signal of the converter is not that easily understood. Therefore, an average model can be used for control design purposes, as the dynamics of the average values are of more interest than the dynamic of the instantaneous values. In addition, the average model allows the use of a modulating signal to control the switches, permitting higher time steps and is thus faster to simulate.

The average model represents the voltage source converter through three voltage sources generating the AC voltage at the output of the converter, averaged over one cycle of the switching frequency. The model does not require gate signals, but is instead supplied a reference signal for the AC voltage.

3.2 Pulse Width Modulation

The converter provides conversion from direct voltage at the input to a sinusoidal alternating voltage at the output [20]. Both the magnitude and frequency of the alternating voltage output is determined by the converter. This is achieved by controlling the set of switches to be turned on and of through pulse width modulation (PWM). The inverter is composed of three legs, one for each phase, as shown in Figure 1. Each leg contains two sets of switches in parallel with a diode. Only one of the two sets of switches in each leg is turned on at the same time.

In pulse width modulation, a reference sinusoidal signal with the desired frequency is compared with a triangular waveform with frequency equal to the switching frequency. The switch duty ratio, the time ratio of when the switches in the inverter is turned on and off, is based on this comparison. When the reference signal is greater than the triangular waveform the upper set of switches in the converter leg is switched on. When the reference signal is less than the triangular waveform the lower set of switches in the inverter leg is turned on.

Each leg of the three-phase voltage source converter has a reference signal, displaced in phase angle by 120° from each other. The output of the voltage source converter will be an alternating signal with fundamental frequency equal to the frequency of the reference signals and harmonics around positive integer multiples of the switching frequency. The working principles of pulse width modulation for a three-phase voltage signal are shown in Figure 2.

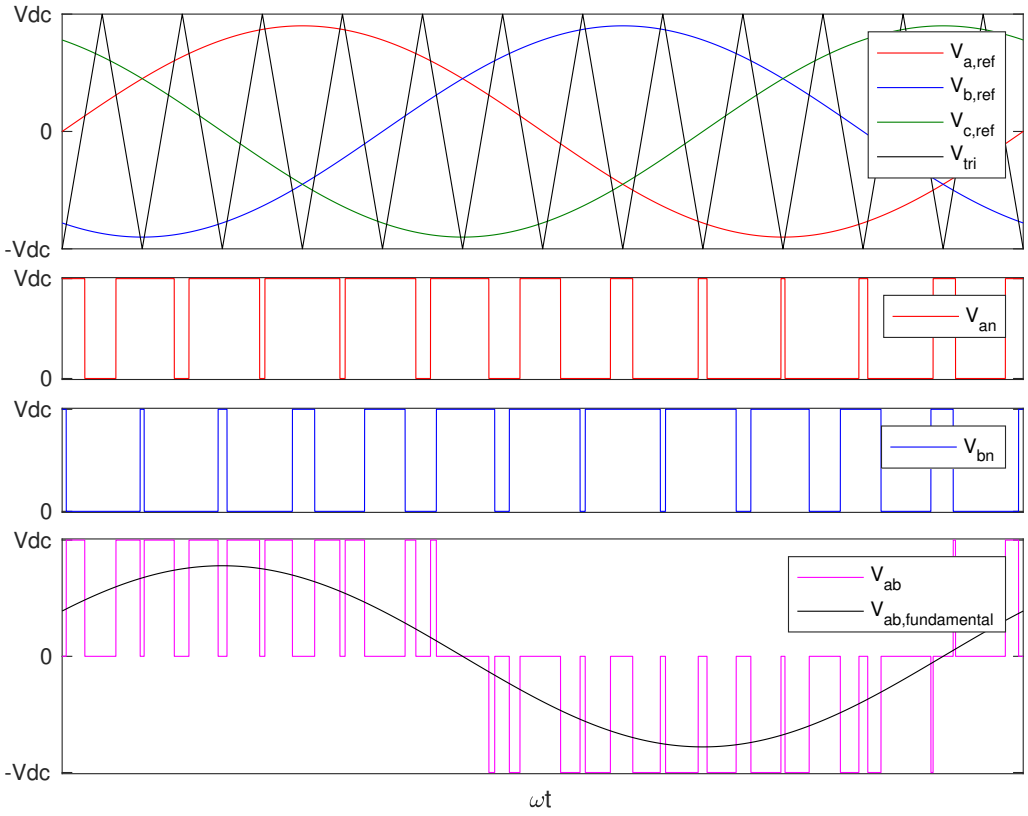

Figure 2: Switching scheme of a three-phase voltage source converter.

In an average model, the input to the voltage source converter is the reference voltage signal. The reference signals are defined as in Equation (1). The m is the modulation index which describes the ratio between the peak values of the reference signal, $\hat{V}_{ref}$, and the triangular waveform, $\hat{V}_{tri}$, as shown in Equation (2).

$$v_{ref} = m \cdot v_{dc} \sin \omega t \tag{1}$$

$$m = \frac{\hat{V}_{ref}}{\hat{V}_{tri}} \tag{2}$$

The modulating index should be in the range $0 < m < 1$. Exceeding this range will cause overmodulation which will result in more harmonics in the output. The range of the modulating index limits the amplitude of the fundamental frequency output. However, by applying space vector modulation, the modulation index can increase beyond 1 without having overmodulation [21]. This will enable the voltage output to be higher compared to the input direct voltage than PWM without space vector modulation.

Space vector modulation builds on the fact that there are only eight possible switching combinations for a three-phase inverter. Two of these switching states will result in short-circuits at the output, and thus are referred to as zero space vectors. The other six switching states defines the six other space vectors, 60° displaced from each other in phase angle. At any time, the desired output voltage vector can be formed by summation of a number of these vectors. This will result in a maximum possible magnitude equal to $\frac{2}{\sqrt{3}} v_{dc}$, thus allowing the modulating signal to increase its range to $0 < m < \frac{2}{\sqrt{3}}$. The only

difference from regular PWM is the positions of the zero space vectors. In regular PWM these are predefined and fixed while for space vector modulation they are undefined. Thus, they can be manipulated to give harmonic benefits.

The space vector modulation reference waveforms for the three legs of the inverter can be generated by continuously adding a triangular varying offset signal to the set of three-phase sinusoidal voltage references, centered around zero at all times. The mathematical expression describing the space vector modulation signal is shown in Equation (3) where $v_{ref(SVM)}$ is the space vector modulation reference signals and v_{ref} is the sinusoidal voltage references. The max/min expression result in the offset signal centered around zero. The three-phase sinusoidal voltage references, the offset signal and the resulting space vector modulation reference signals are shown in Figure 3.

$$v_{ref(SVM)} = v_{ref} - \frac{1}{2}\left[max(v_a, v_b, v_c) + min(v_a, v_b, v_c)\right] \tag{3}$$

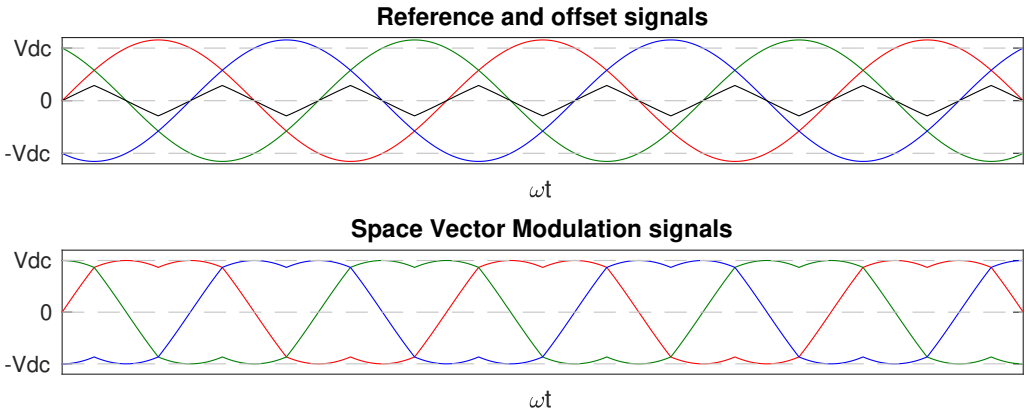

Figure 3: Reference modulating signals applied offset to gain the Space Vector Modulation signals.

3.3 Control loops

The control of the voltage source converter includes multiple control loops [13]. The control system is made up of an inner current control loop and an outer control loop to control either the voltage or power of the converter. In addition, the control system includes a Phase-Locked Loop (PLL) to ensure that the frequency and phase angle of the voltage source converter output matches those of the grid.

3.3.1 Reference frame transformations

The control of the voltage source converter is generally implemented using space vector representation in the synchronous rotating frame, also referred to as the dq-frame. This representation projects the space vector onto two orthogonal axes which rotate with angular frequency corresponding to that of the transformed signal. The dq-frame representation is achieved through first Clark transformation and then Park transformation.

Clark transformation
The Clark transformation, also known as the $\alpha\beta$-transformation, converts the representa-

tion of a three-phase signal, in the natural *abc*-frame, into space vectors in the Cartesian coordinate system without loosing any information regarding magnitude and phase of the signal. The transformation will reduce the number of signals from three to two, which also reduces the complexity. The transformation of a three-phase current signal into the $\alpha\beta$-frame is shown in Equation (4) [13].

$$\begin{bmatrix} i_\alpha \\ i_\beta \\ i_0 \end{bmatrix} = \frac{2}{3}\boldsymbol{C}\begin{bmatrix} i_a \\ i_b \\ i_c \end{bmatrix} = \frac{2}{3}\begin{bmatrix} 1 & -\frac{1}{2} & -\frac{1}{2} \\ 0 & \frac{\sqrt{3}}{2} & -\frac{\sqrt{3}}{2} \\ \frac{1}{2} & \frac{1}{2} & \frac{1}{2} \end{bmatrix}\begin{bmatrix} i_a \\ i_b \\ i_c \end{bmatrix} \tag{4}$$

Park transformation

The Park transformation converts the signals from the stationary orthogonal $\alpha\beta$-frame to the rotating synchronous *dq*-frame. The Park transformation is described through Equation (5).

$$\begin{bmatrix} i_d \\ i_q \end{bmatrix} = \boldsymbol{P}\begin{bmatrix} i_\alpha \\ i_\beta \end{bmatrix} = \begin{bmatrix} \cos(\omega t) & -\sin(\omega t) \\ \sin(\omega t) & \cos(\omega t) \end{bmatrix}\begin{bmatrix} i_\alpha \\ i_\beta \end{bmatrix} \tag{5}$$

As can be seen from Equation (5), the Park transformation phase shifts the $\alpha\beta$-frame with angle $\theta = \omega t$. This gives the relation between current and voltage in $\alpha\beta$-frame and *dq*-frame as shown in Equation (6):

$$\begin{aligned} i_{dq} &= i_{\alpha\beta} \cdot e^{-j\theta} \\ v_{dq} &= v_{\alpha\beta} \cdot e^{-j\theta} \end{aligned} \tag{6}$$

To reverse the Park and Clark transformation, the inverse matrices $\boldsymbol{C}^{-1}$ and $\boldsymbol{P}^{-1}$ are applied as shown in Equation (7) and (8). Collective reverse transformation from *dq*-frame to natural *abc*-frame can mathematically be expressed as in Equation (9).

$$\begin{bmatrix} i_\alpha \\ i_\beta \end{bmatrix} = \boldsymbol{P}^{-1}\begin{bmatrix} i_d \\ i_q \end{bmatrix} \tag{7}$$

$$\begin{bmatrix} i_a \\ i_b \\ i_c \end{bmatrix} = \boldsymbol{C}^{-1}\begin{bmatrix} i_\alpha \\ i_\beta \\ i_0 \end{bmatrix} \tag{8}$$

$$\begin{bmatrix} i_a \\ i_b \\ i_c \end{bmatrix} = \begin{bmatrix} \cos(\omega t) & -\sin(\omega t) & 1 \\ \cos\left(\omega t - \frac{2\pi}{3}\right) & \sin\left(\omega t - \frac{2\pi}{3}\right) & 1 \\ \cos\left(\omega t + \frac{2\pi}{3}\right) & \sin\left(\omega t + \frac{2\pi}{3}\right) & 1 \end{bmatrix}\begin{bmatrix} i_d \\ i_q \\ i_0 \end{bmatrix} \tag{9}$$

The relationship between the $\alpha\beta$-frame and the dq-frame is shown in Figure 4. The figure shows that the dq-frame is rotated by an angle θ from the $\alpha\beta$-frame. The abc-frame voltage and current vectors, V and I, are also added to the figure, displaced by an angle of φ.

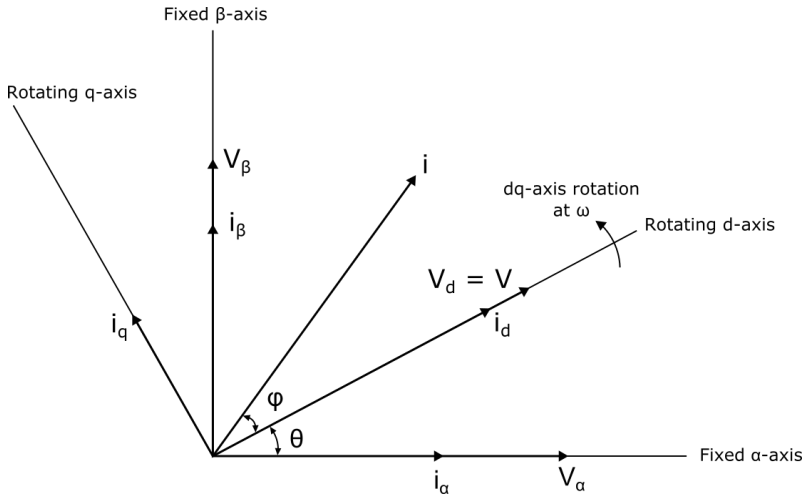

Figure 4: Voltage and current vectors shown as $\alpha\beta$- and dq-components. Figure adapted from [22].

3.3.2 Phase locked loop

To achieve that the output signals from the converter are synchronized with the conditions of the microgrid, a Phase-Locked Loop (PLL) is included in the control loops of the converter. The PLL is a closed loop that synchronizes the frequency and phase angle of the output signal. The PLL consists of a phase detector block, loop filtering through a proportional integral (PI) controller and a voltage controlled oscillator (VCO). The PLL is usually implemented in the synchronous reference frame. The block-diagram of the PLL control loop is shown in Figure 5.

The measured voltage signal at the converter output is transformed into d- and q-components. The angle difference between the components is then passed through the PLL loop. The loop continues until the components are synchronized, which correlate with the d-component aligning with the converter output voltage and q-component being reduced to zero.

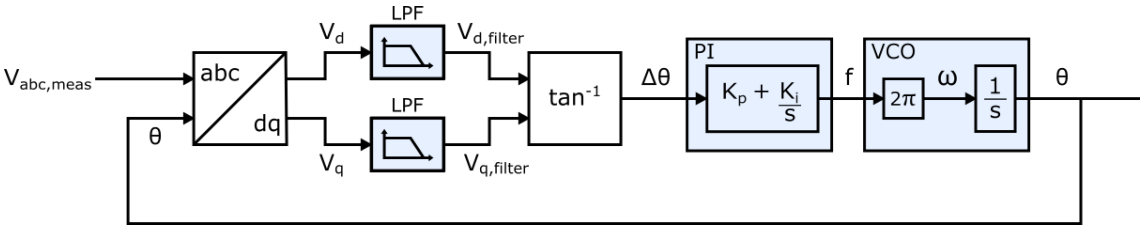

Figure 5: PLL control loop of the voltage source converter.

To determine the values of the PI controller constants, K_p and T_i, the loop is tuned by the symmetrical optimum criteria. This criteria is used since the open-loop transfer function of the PLL loop has two poles at the origin, as can be shown in the expression for the open-loop transfer function of the PLL control loop in Equation (10). Symmetrical optimum is

obtained by finding the maximum phase angle at the crossover frequency of the open-loop transfer function. The tuning criteria of symmetrical optimum is determined by imposing maximum phase angle at the crossover frequency, as shown in Equation (11).

$$G_{PLL,OL}(s) = K_p \frac{1 + T_i s}{T_i s} \cdot \frac{1}{T_f s + 1} \cdot \frac{2\pi}{s} \tag{10}$$

$$\begin{cases} |G_{PLL,OL}(j\omega_c)| = 1 \\ max(\angle G_{PLL,OL}(j\omega)) = \angle G_{PLL,OL}(j\omega_c) \end{cases} \tag{11}$$

The time constant of the PI controller is set to be bigger than the time constant of the filter. This can be expressed as $T_i = a^2 T_f$, where a and T_f can be chosen freely and thus provide two degrees of freedom. From the criteria of symmetrical optimum, the constants of the PI controller in the PLL control loop can be tuned with K_p and T_i as in Equation (12) and (13).

$$K_p = \frac{1}{2\pi T_f a} \tag{12}$$

$$T_i = a^2 T_f \tag{13}$$

3.3.3 Current controller

The inner loop current control eliminates deviations in the measured current at the converter output from the reference current, and create voltage reference signals for the pulse-width modulation. The current control is based on Kirchhoff's voltage law which gives the relation between the converter output voltage and the grid voltage.

$$\begin{aligned} L\frac{di_a}{dt} + Ri_a &= e_a - v_a \\ L\frac{di_b}{dt} + Ri_b &= e_b - v_b \\ L\frac{di_c}{dt} + Ri_c &= e_c - v_c \end{aligned} \tag{14}$$

As stated in Section 3.3.1, the control of voltage source converters is usually presented in the synchronous reference frame. This allows the number of control components to be reduced from three to two. The Clark transformation reduces the *abc*-components to the two α- and β-components. These components are then given a rotation through the Park transformation. The relationship between the voltage and current components in $\alpha\beta$- and dq-frames is shown in Equation (15).

$$\begin{aligned} i_{dq} &= i_{\alpha\beta} \cdot e^{-\theta} \\ v_{dq} &= v_{\alpha\beta} \cdot e^{-\theta} \end{aligned} \tag{15}$$

When the Clark transformation and the relationship shown in Equation (15) are applied to the set of expressions in Equation (14), the two expressions in Equation (16) are obtained.

The equations show that the two expressions are now coupled, due to the derivative term across the line inductor.

$$\begin{aligned} L\frac{di_d}{dt} + Ri_d - \omega L i_q &= e_d - v_d \\ L\frac{di_q}{dt} + Ri_q - \omega L i_d &= e_d - v_q \end{aligned} \tag{16}$$

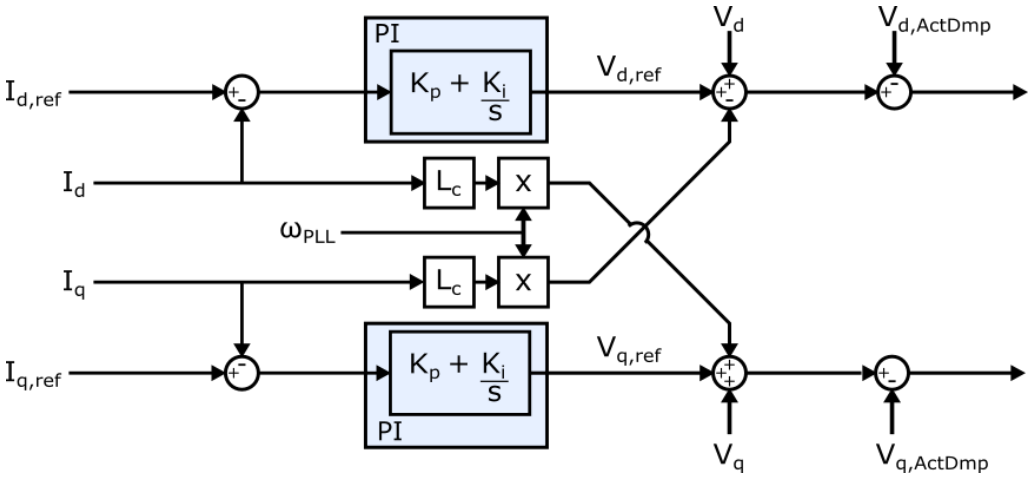

Figure 6: Current control loop of the voltage source converter.

The outputs from the current control loop shown in Figure 6 are the voltage reference signals v_d and v_q. These outputs are then divided by v_{dc} which result in the modulating reference signals for the PWM.

The parameters in the PI controllers can be determined through modulus optimum. This takes root in the transfer function of the current control, which is expressed through Equation (17). The proportional constant K_p and the first fraction containing the time constant T_i represent the PI controller. The second fraction represent the output filter of the converter, defined by the filter resistance r and induction l, and the last fraction represent a time delay with time constant T_{sum}. The internal current control loop should be designed to achieve fast response [22].

$$G_{CC,OL}(s) = K_p \frac{1 + T_i s}{T_i s} \frac{1}{r\left(1 + \frac{l}{r}s\right)} \frac{1}{1 + T_{sum}s} \tag{17}$$

Modulus optimum is chosen as the tuning approach as it is applicable in the presence of a single dominant pole at the origin. The slowest pole is canceled by fixing T_i to be equal to l/r. The open-loop transfer function will then be reduced to that of Equation (18). The reduced open-loop transfer function is used to find the closed-loop transfer function (19).

$$G_{CC,OL}(s) = \frac{K_p}{l \cdot s} \frac{1}{1 + T_{sum}s} \tag{18}$$

$$G_{CC,CL}(s) = \frac{G_{CC,OL}}{1 + G_{CC,OL}} = \frac{K_p}{l \cdot T_{sum}} \frac{1}{s^2 + \frac{1}{T_{sum}}s + \frac{K_p}{l \cdot T_{sum}}} \tag{19}$$

Based on the damping Equation (20), the damping coefficient is imposed to be $\zeta = \frac{1}{\sqrt{2}}$. Comparing (19) and (20) gives the two relations in Equation (21) and (22).

$$s^2 + 2\zeta\omega_n s + {\omega_n}^2 \tag{20}$$

$$\omega_n = \sqrt{\frac{K_p}{l \cdot T_{sum}}} \tag{21}$$

$$2\zeta\sqrt{\frac{K_p}{l \cdot T_{sum}}} = \frac{1}{T_{sum}} \longrightarrow K_p = \frac{1}{4 \cdot {T_{sum}}^2\zeta^2} l \cdot T_{sum} = \frac{l}{2 \cdot T_{sum}} \tag{22}$$

3.3.4 DC voltage controller

The current control regulates the real and reactive power output of the converter on the AC side. The output from the current controller is based on the DC side voltage being impressed by an ideal DC voltage source, and that the voltage source converter supply bidirectional power exchange. This is, however, not always the case. Some examples of this is for Photo-voltaic (PV) systems, as well as variable-speed wind turbine generator sets, fuel-cell units, and gas turbine generator sets. In these cases the DC side voltage is impressed by a DC power source, which may vary in time, and it is thus necessary to regulate the DC side voltage. This can be done with an outer DC voltage control loop.

To define the DC voltage control, real power equality between the AC and DC side of the voltage source converter is imposed. The real power at the AC side can be expressed as $P = \frac{3}{2}(v_d i_d + v_q i_q)$ in the dq-frame, where v_d, v_q, i_d, and i_q are the d- and q-components of the AC side voltage and current of the converter. In steady state the last term can be eliminated as $v_q = 0$. Power equality between the AC and DC side can thus be expressed as shown in Equation (23), where it is assumed that there is no losses across the converter.

$$P_{dc} = P_{ac} \longrightarrow v_{dc} i_{dc} = -\frac{3}{2} v_d i_d \tag{23}$$

From Equation (23) the DC side current, i_{dc}, can be expressed as in Equation (24).

$$i_{dc} = -\frac{3}{2}\frac{v_d i_d}{v_{dc}} \tag{24}$$

As the DC side voltage is linked to the dynamics of the DC side capacitance, the DC side voltage can be expressed as in Equation (25), substituting i_{dc} with the term found in Equation (24). The i_s is the current from the DC side power source and C is the capacitance of the DC side capacitance.

$$\frac{dv_{dc}}{dt} = \frac{1}{C}(i_{dc} - i_s) = \frac{1}{C}\left(-\frac{3}{2}\frac{v_d i_d}{v_{dc}} - i_s\right) \tag{25}$$

Equation (25) can be linearized around the operating point, given by the values v_{dc0},v_{d0}, i_{d0} and i_{s0}, which result in Equation (26). To achieve the linearization, the instantaneous value of each of the variables are defined as the value of the variable at the operating point

added a deviation. This is shown in the general form as $x_i = x_{i0} + \Delta x_i$. Since it is the relation between v_{dc} and i_d that is of interest, the other terms in the linearized expression is addressed as a disturbance δ, shown in Equation (27).

$$\frac{d\Delta v_{dc}}{dt} = -\frac{1}{C}\left(\frac{3}{2}\frac{v_{d0}}{v_{dc0}}\Delta i_d + \frac{3}{2}\frac{i_{d0}}{v_{dc0}}\Delta v_d - \frac{3}{2}\frac{v_{d0}i_{d0}}{v_{dc0}^2}\Delta v_{dc} + \Delta i_s\right) \tag{26}$$

$$\frac{d\Delta v_{dc}}{dt} = -\frac{1}{C}\left(\frac{3}{2}\frac{v_{d0}}{v_{dc0}}\Delta i_d + \delta\right) \tag{27}$$

From the Equation (27), the dependency of v_{dc} on i_d can be described through Equation (28). The DC voltage control is modeled with a PI controller and a constant that invert the sign of the signal as shown in Figure 7. $V_{dc,ref}$ is the reference value for the voltage on the DC side of the converter, V_{dc} is the measured value and $I_{d,ref}$ is the d-axis current reference for the current control loop.

$$\Delta v_{dc} = -\frac{\frac{2}{3}\frac{v_{d0}}{v_{dc0}}}{sC}\Delta i_d \tag{28}$$

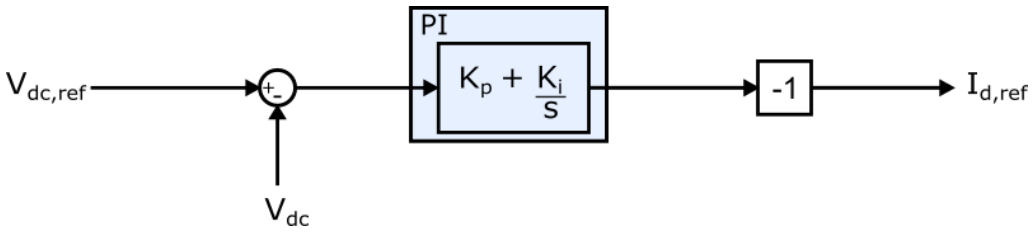

Figure 7: DC voltage control of the voltage source converter.

The parameters in the PI controllers can be determined through symmetrical optimum, where the main goal of the tuning is to achieve optimal regulation and stability. Tuning through symmetrical optimum is obtained through the transfer function of the voltage controller. The open-loop transfer function of the DC voltage controller contains the relation between the DC voltage and d-axis current in Equation (28), and an equivalent first order equivalent of the current control loop. The first order equivalent transfer function of the current control loop can be obtained by imposing equal integral of error between the step response of the second order transfer function of the current control and the first order equivalent transfer function, as shown in Equation (29). The result is a first order transfer function with time constant $T_{eq} = 2T_{sum}$, where T_{sum} was defined in Section 3.3.3.

$$\int_0^\infty \epsilon_{CC,CL}dt = \int_0^\infty \epsilon_{CCEQ,CL}dt \tag{29}$$

The transfer function of the voltage controller is shown in Equation (30). The K_p and T_i are the parameters of the PI controller, T_{eq} is the time constant of the equivalent transfer function of the current control, v_{d0} and v_{dc0} are the d-component and DC voltages of the converter at steady state operating conditions, and C is the DC side capacitance. For simplicity, the parameters $K = \frac{3}{2}\frac{v_{d0}}{v_{dc0}}$ and $T_c = \frac{1}{\omega_b C_{pu}}$ are defined. The parameters ω_b is

the base frequency and C_{pu} is the per unit DC side capacitance.

$$G_{Vdc,OL}(s) = K_p \frac{1+sT_i}{sT_i} \frac{1}{1+sT_{eq}} \frac{3}{2} \frac{v_{d0}}{v_{dc0}} \frac{1}{sC} \tag{30}$$

For symmetrical optimum, the T_i cannot be chosen equal to T_{eq} to achieve pole cancellation as the system would then be unstable. Tuning according to symmetrical optimum is obtained from imposing maximum phase angle at crossover frequency as shown in Equation (11) in Section 3.3.2. Maximum phase angle occurs at $\omega_c = \frac{1}{\sqrt{T_i T_{eq}}}$. From this, the tuning criteria for the time constant of the controller is as in Equation (31).

$$T_i = T_{eq} \left(\frac{1+\sin\phi_{max}}{1-\sin\phi_{max}} \right) \tag{31}$$

The transfer function will have its maximum phase ϕ_{max} symmetric around $\frac{1}{T_i}$ and $\frac{1}{T_{eq}}$. By symmetric properties the T_i can thus be described as $T_i = a^2 T_{eq}$, where a is the symmetrical difference between $\frac{1}{T_i}$ and $\frac{1}{T_{eq}}$ and ω_c. The gain parameter K_p is found from the magnitude criteria of the Nyquist stability criteria and is expressed in Equation (32). The variable a is a degree of freedom.

$$K_p = \frac{T_c}{K T_{eq} a} \tag{32}$$

4 Synchronous generator system

For synchronization purposes, a synchronous machine is added to the microgrid models used in this thesis to make sure there is an inertia component present. This is of interest as it adds a criteria to the synchronization strategy. Since converter-based generation does not have inertia present, the output of the converter can abruptly change its operating point without problems. Inertia components, however, can not instantaneously change their operating point. This requires a larger time period for the synchronization process.

A synchronous generator system consists of a synchronous machine generating an alternating three-phase voltage to supply power to a load or a grid. The voltages at the generator terminals are produced by a rotating electromagnetic field which induces voltages in the stator windings of the machine. The rotating field is produced by a DC field current applied to the machine rotor by the excitation system. The field produced by the DC field current rotates due to the rotor axis being connected to a turbine prime mover. The prime mover of synchronous generators can run on fossil fuels such as gas, oil, coal and nuclear fuel, or it can run with hydro power. The synchronous generator system also includes a governor which controls the operation of the machine through regulating the fuel inlet to the turbine system. The generator system is schematically shown in Figure 8.

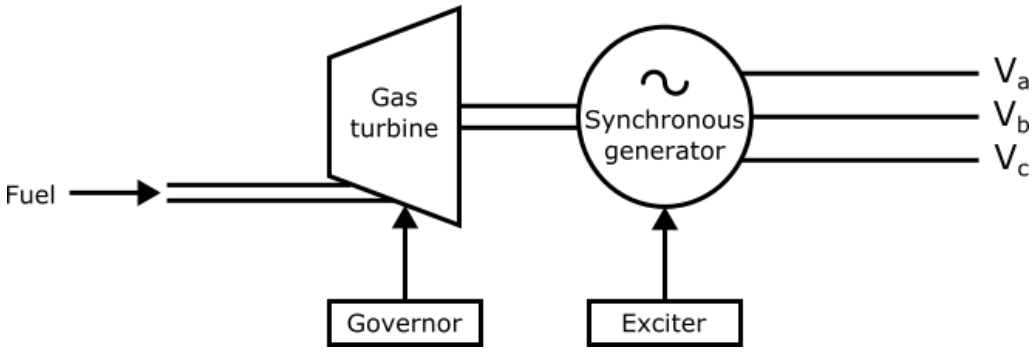

Figure 8: Synchronous generator system with gas turbine prime mover.

The reason for the name synchronous generator is because the machine operates at a speed that is directly proportional to the grid frequency. This can be shown through Equation (33), where the frequency of the induced voltage in the stator windings, f, is equal to the speed of the rotor in rounds per minute (rpm), n_s, multiplied by the number of poles on the rotor, P, and divided by 120 [23].

$$f = \frac{P}{120} n_s \tag{33}$$

This means that if the frequency in the grid increases, the speed of the synchronous generator will also increase, and when the frequency decreases, the speed of the synchronous generator will decrease. The grid frequency should be kept at the nominal frequency of 50 Hz. The frequency in the grid is determined by the balance between power generation and load demand.

The induced voltage in the generator stator windings is a function of the flux generated by the rotor current, as seen in Equation (34). The induced sinusoidal voltage, E, has an amplitude of $N\omega_s\Phi$, where N is the number of turns in the stator winding, ω_s is the synchronous speed of the rotor in rad/s and Φ is the flux generated by the rotor field current.

$$E = N\omega_s\Phi \sin \omega_s t \tag{34}$$

The number of turns in the stator winding is constant, and the synchronous speed of the rotor follows the grid frequency. Thus, to control the output voltage of the generator the flux in the machine can be regulated. Since the flux is generated from the field current in the rotor, the voltage at the output terminals is a function of the field current. Thus, the synchronous generator can contribute to maintaining the nominal voltage of the grid by regulating the field current.

4.1 Synchronous inertia and frequency stability

Synchronous generators play a huge role in the frequency stability aspect of a grid. Synchronous generators have mechanical inertia and are thus capable of storing kinetic energy in their rotating mass [24]. As the terminals of the synchronous generators are directly linked to the grid, the stored energy in the generators' rotating mass can be exchanged with

the grid during disturbances. Thus, it makes the grid less vulnerable towards frequency fluctuations caused by imbalances between generation and load.

In an AC power system the rotational speed of the synchronous machine follows the grid frequency, as was described in Equation (33). Consequently, the total mechanical inertia stored in the synchronous machine will not only offer some resistance to a change in the rotational speed, but will also oppose changes in frequency of the induced voltage in the machine. Because of this inertia characteristic of synchronous generators, they are considered a key element in maintaining a reliable operation of the power system.

The mechanical dynamics of synchronous generators are governed by the swing equation, which can be expressed as in Equation (35). The parameter f represents the frequency at the machine terminals, the P_m and P_e are the mechanical and electric power of the machine, and H is a the inertia constant used to quantify the inertia of the machine. The equation is expressed in per unit value, with the nominal frequency of 50 Hz as the base value, and it is assumed small frequency deviations from the rated value. The equation shows that the inertia, H, of the synchronous machine express resistance to a change in the frequency that results in a power imbalance between the mechanical and electrical power.

$$2H\frac{df}{dt} = P_m - P_e \tag{35}$$

The inertia constant indicates how many seconds the generator can provide its rated power, only based on its stored kinetic energy. Mathematically, the inertia constant can be described as shown in Equation (36), where J is the moment of inertia, ω_n is the rated rotational speed in rad/s, S is the rated apparent power, and E_k denotes the kinetic energy of the rotating parts of the machine.

$$H = \frac{\frac{J\omega_n^2}{2}}{S} = \frac{E_k}{S} \tag{36}$$

The concept of inertia of a single synchronous generator can be used to explain the total inertia of an AC power system, often consisting of a large number of parallel synchronous generators. The swing equation shown in Equation 35 can be used to express the dynamics of all generators in the system, where the inertia constant represent the total inertia of the system and the mechanical power P_m and electrical power P_e are set to represent the total generated power and the total load in the grid.

The inertia of the power system plays a huge role when it comes to the reliability of the grid. The frequency of the grid is governed by the balance between generation and load. Thus, large load increases and decreases or faults at a generating unit, resulting in loss of generation, can cause frequency fluctuations. The power of inertia, where the kinetic energy of the rotating machines resist sudden changes in frequency, provides the grid time to reestablish the balance between the generation and the load demand.

4.2 Gas turbine governor modeling

There exists multiple models to represent the governor system and prime mover of a synchronous generator. In this thesis, a gas turbine governor model is used as part of the synchronous generator system to validate the proposed synchronization technique. The

model in this thesis is adapted from the much used IEEE's GGOV1 gas turbine model, which is more described in [25] and [26]. The gas turbine model consists of a compressor, a combustion chamber and a turbine that supplies mechanical power to the synchronous generator. The mechanical power is regulated by the turbine governor.

The gas turbine model is governed by speed control. This is essential since the speed of the prime mover is directly linked to the frequency of the voltage output of the synchronous generator. The speed control follows a defined speed reference, and subtract the measured speed of the synchronous machine. The speed deviation is added to a droop signal, which is a feedback signal multiplied by a droop coefficient that represents the droop of the machine. The IEEE model also include a load controller as an outer loop to the speed control, which adjusts the speed set point to control the power towards a preset value. The load control is not included in the model used in this thesis.

In this thesis, the droop control of the synchronous machine is not activated. The reason for this is that the microgrid models used in the simulation only consist of one synchronous generator. Droop control is not essential with only one synchronous machine in the microgrid as droop control is used for power sharing among parallel synchronous generators. However, the absence of droop control may be noticeable when the two grids are working in grid-connected mode and there is a change in load or generation. For the simulations performed in this thesis, the scope is to evaluate the synchronization process leading up to the interconnection of two microgrids and shortly after to see the effect of the transition from islanded to grid-connected operation. Each microgrid is able to supply its local load with the generation produced locally in each grid. When interconnected, the load is still kept the same and thus there is no need to have power sharing of changes in the load. To include the droop control in the simulations might have been relevant if one were to study the case of synchronizing and interconnecting the two microgrids with the motivation that one of the microgrids need power support from the other.

The speed deviation signal from the speed control is passed through a PID controller and is applied as input to a "low value select" block. This "low value select" block is the overall control block. It chooses the most limiting control signal to control the fuel valve in the turbine system. The other inputs to this block in the IEEE GGOV1 gas turbine model are signals from acceleration control and temperature control.

The acceleration control included in the general model from IEEE is deactivated in the model used in this thesis. It is presumed that the synchronous generator runs under normal operation when the synchronization process happens. That means that start-up and shut-down of the synchronous generator are not considered. Start-up and shut-down of the synchronous generator are mainly the target for the acceleration control to prevent large changes in the generator operation [26].

The goal of the temperature control is to protect the hot sections of the turbine from over-heating. It limits the amount of fuel fed into the turbine system to prevent over-heating of the combustion cans, transition ducts, and nozzles on the turbine. The temperature control is activated in the simplified model used in this thesis. The temperature control loop is limited to supply the "low value select" block with a "base load" which is the maximum output mechanical power the turbine system can achieve without the risk of over-heating.

The output of the "low value select" block is the control signal given to the main fuel valve which regulates the amount of fuel fed to the turbine system. The turbine system includes the fuel system and the turbine. The fuel system is defined by the actuator lag and has

limits to its output and flow rate. It also includes a fuel flow supplement, W_{fnl}, to ensure that the turbine rotates in no load conditions. The turbine is modeled by a turbine gain and lag that provide the mechanical power output fed to the synchronous generator.

A schematic of the adapted IEEE GGOV1 gas turbine governor model used in this thesis is shown in Figure 9.

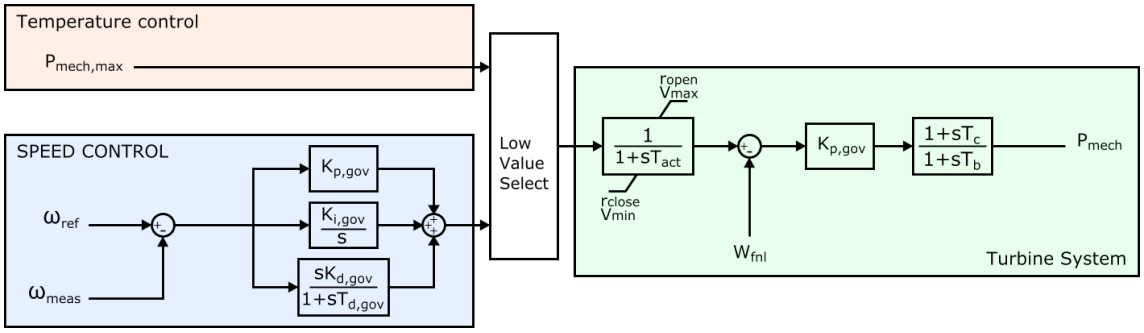

Figure 9: Block diagram of the gas turbine governor model used in this thesis.

4.2.1 Choice of prime mover governor model

The initial idea for the governor model of the synchronous generator was a gas turbine governor model. The reason was that the microgrid model used for the simulations, provided by SINTEF, included a gas turbine synchronous generator model. During the thesis work, the question was raised if using a gas turbine model would be the most relevant choice. The IEEE GGOV1 gas turbine model is originally intended for much larger generator systems, ranging from 1 MW and above, than was intended for the model to be used in this thesis.

As gas turbines are more generally used for much larger power plants, a microturbine system was considered. They are more frequently used for smaller power generating units. However, a microturbine have much higher rotational speed than a traditional gas turbine. This would require the microturbine to be connected to the grid through a power converter to acquire the nominal grid frequency. Thus, the point of adding a synchronous generator to the model simulation disappears as there would be no synchronous machine with rotational inertia directly connected to the grid.

Other synchronous turbine models were considered, such as diesel engines and hydro power plants. Both options are relevant applications in a rural microgrid. Through conversations with SINTEF, it was concluded that using the IEEE GGOV1 gas turbine model would be sufficiently accurate. The model includes per unit values and by reducing the base values for the microgrid model it would give justifiable results. However, there might be differences in some parameters, such as the inertia constant and the synchronous generator reactances, in small machines compared to larger machines.

5 Synchronization control method

As mentioned in Section 2.1, there are some general characteristics to microgrid control methods. The control of microgrids is usually divided into a hierarchical structure with the three layers primary, secondary and tertiary. The focus of this thesis is on the task of

synchronizing the microgrid to an external grid, which is included in the secondary control level. Different control strategies for microgrids can be categorized with either a centralized, a decentralized or a distributed control approach, where the level of communication between grid units characterize the different approaches.

The purpose of this thesis is to propose a synchronization strategy for microgrids. The synchronization strategy proposal is based on a master-slave control technique with a microgrid central controller at the connection point to an external microgrid. At the central controller, synchronization control loops are added to align the operating points of the connecting grids. For simplicity, this thesis focuses on two microgrids that are to interconnect. The microgrids include both a synchronous generator and generation from a converter-based unit that provide a local load. As discussed in Section 2.2, the operating point of a microgrid may deviate from nominal values of frequency, voltages and phase angles due to more intermittent generation from renewable energy sources and unpredictable load variations. Thus, before interconnection, these values need to be aligned between the two microgrids to prevent large inrush currents.

This section presents the work completed throughout the thesis work and the proposed synchronization strategy for microgrid interconnection. The methods used to find the controller gains of the proposed synchronization loops are also recorded in this section.

5.1 Literature review on synchronization methods

Synchronization of several microgrids to form a multigrid configuration is a relatively new research field. The majority of articles on microgrid synchronization address reconnection to strong utility grids. On the topic of synchronization control loops for microgrids, strategies that employ PI controllers to create offset signals for frequency, phase angles and voltage magnitudes are widely used.

In [16], a microgrid with both converter-based and synchronous generators is synchronized with the utility grid. The synchronization is performed by the synchronous generator, where frequency offset signals are added to the speed reference of the synchronous generator governor. It is assumed that the voltages in the two grids are both kept close enough to 1 pu, and that the deviation in phase angles is the dominating factor. The phase deviation between the two grids are measured through phase measurement units and is fed through a PI controller. The PI controller output is then added to the speed reference for the synchronous generator governor. As a result of this added offset signal, the generator will speed up or slow down to eliminate phase angle deviations.

In [27], the task is to synchronize a virtual synchronous machine to a grid. As the virtual synchronous machine mimics the dynamics of a synchronous machine, the chosen synchronization strategy is similar to strategies used to synchronize these. The authors assume that the deviation in voltage magnitudes can be neglected and propose a synchronization loop that eliminates deviations in frequency and phase angle. The synchronization loop includes PI controllers for both the frequency and the phase angle deviation. The synchronization control signal is then applied to the frequency droop control of the virtual synchronous machine.

The authors of [28] look at the synchronization of a microgrid, with strictly converter-based generation, to be connected to the utility grid. The proposed strategy includes a central main controller at the connection point which calculates the deviations in frequency, voltages and phase angles. The deviations are sent to local controllers at all converter units

where phase and voltage deviations are passed through PI controllers. The output of the PI controllers are then added to the existing droop control loops of the converters.

The microgrid studied in [29] includes both converter-based and synchronous generating units. Here the task of reaching synchronization with the external utility grid is divided between several of the controllable units. The phase angle, frequency and voltage deviations are calculated in an intelligent electronic device situated at the connection point. The deviations are passed through PI controllers in the microgrid central controller to create offset signals. The frequency and voltage offset signal are then divided between the controllable units and multiplied by a weighting factor. The frequency offsets are also passed through frequency filters that suits the dynamics of each unit. The phase angle offset is added to the frequency offset signal when the frequency deviation of the system is less than 0.01.

5.2 The synchronization strategy

In the case of a microgrid connecting to the utility grid, it is evident that the microgrid with weaker grid characteristics should synchronize to the stronger utility grid. In the case of interconnecting two microgrids, however, both of the grids that are to be interconnected have weak characteristics. This raises a question as to which microgrid should synchronize to which, or if they both should synchronize towards a common reference point. The most evident option might be to synchronize the grid with the lowest rated power to the larger one, if there is a size difference. The question of which microgrid that is to be synchronized needs to be addressed when designing a synchronization control strategy, especially in cases where more than two microgrids are to interconnect to form a multigrid configuration. With more than two microgrids, it might not be obvious which grid should synchronize and to what operating conditions the grid should synchronize to.

The proposed synchronization strategy in this master thesis is centered around synchronizing the grid with the lowest power rating to match the operating point of the larger grid. The choice of synchronizing only one microgrid instead of both is done because it is convenient. Since the microgrids are weak grids, they are easily subjected to disturbances which complicate the synchronization process. Therefore, it will be less complicated to limit the synchronization process to address only one of the microgrids. Another reason for synchronizing only one microgrid is that if the two microgrids constantly are trying to match each other's operating point, there might be more oscillations around synchronized state. This might cause it to take longer time to reach synchronization.

The aim of the proposed synchronization loops is to eliminate the deviations in phase angle and frequency between the two microgrids. The synchronization control signals will be served as an offset to the speed reference for the governor of the synchronous generator in the smallest microgrid. It is assumed that due to requirements to power quality within the microgrids, the voltages are kept close enough to nominal values such that the voltage deviations are not a problem when interconnecting the grids.

As mentioned in Section 2.2, the microgrids will be subject to large inrush currents if they are interconnected without being synchronized in frequency and phase angle within the allowable limits. For the model studied in this thesis, the two microgrids are considered synchronized when the deviation in frequency is smaller than 0.001 pu and deviation in phase angle is smaller than 0.001 rad/s. The allowable deviation limits are adapted from [27].

5.2.1 Master-slave control

For the proposed synchronization strategy a master-slave approach is adapted. This means that there is appointed a master unit which is in charge of defining the set points in voltage and frequency in the microgrid. The other units in the grid operate with control based on local voltage and current measurements. In this case, the master unit is chosen to be the synchronous generator unit. The synchronous generator is thus appointed the task of synchronizing the microgrid upon interconnection with another microgrid. The control of the converter-based generating unit is thus based on local current and voltage measurements at the converter output terminals.

The choice of focusing on the synchronous generator for the synchronization process is based on the fact that the synchronous machine requires a larger time period than the converter to change its operating point. As described in Section 2.2, a synchronous machine will not be able to instantaneously change its operating point due to inertia.

In addition, choosing the synchronous generator to synchronize the microgrid will eliminate the challenge of having the converter switch from grid-forming to grid-following mode when the two microgrids interconnect. The converters can operate constantly in grid-following mode as it is the synchronous generator that controls the set points for voltage and frequency in the microgrids in islanded operation. This approach mimics the thinking of traditional power grids.

The synchronization control loops are added to a microgrid central controller. The synchronization signals are fed to the control system of the synchronous generator through communication links. The master-slave approach will thus only require communication links to one unit which is less complex than a centralized approach where all units participate in the synchronization. However, the reliably of the synchronization process will rely solely on the master unit. Thus, a fault in the master unit or in the communication link to the master unit will effect the availability of the synchronization process. The master-slave approach is schematically shown for the microgrid model in Figure 10.

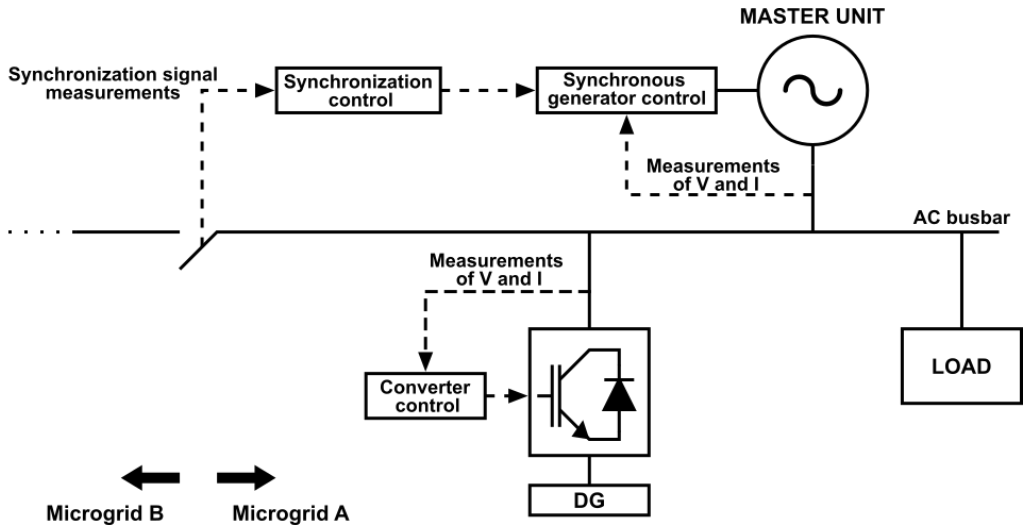

Figure 10: Figure showing the master-slave control implementation in the microgrid.

5.2.2 Proposed synchronization loops

The synchronization control loops are to actively interfere in the operation of the microgrid and synchronize its operating point to that of the connecting grid. As in [27] and [16], the voltage magnitudes of the two systems are assumed to be equal enough to not cause problems when the two grids connect. The focus of the synchronization loops is thus to eliminate deviations in frequency and phase angle between the microgrids.

The inputs to the synchronization loops are the deviations in frequency and phase angle between the two grids. These deviations are calculated from voltage measurements in the two grids, measured at each side of the interconnection switch. The phase angle and frequency of each grid is obtained through phase-locked loops. The corresponding values from each grid are compared to each other to find the deviations. The frequency deviation signal fed to the synchronization control loops is in per unit value, while the phase deviation signal is in real value, rad/s.

Inspired by the articles reviewed in Section 5.1, the proposed synchronization control loops for a multigrid configuration with two interconnecting microgrids are shown in Figure 11. The synchronization loops consist of two parallel PI controller loops, one for the phase angle deviation and one for the frequency deviation. This is adapted from [29]. The outputs of the PI controllers form offset signals in phase angle and frequency. The phase angle offset is added to the frequency offset. The frequency offset is then added to the speed reference for the synchronous generator governor, as is done in [16]. If the synchronization strategy were to include synchronization of voltage magnitudes, a PI controller could be used to produce an offset signal also for the voltage. However, this is not included in this thesis work.

The phase synchronization loop is only activated when the deviation in frequency is less than 0.01 pu. This is because it has no purpose to change the phase angle when the frequency deviation is too large as different frequencies in the two grids forces phase deviation. As the phase angle output of the phase-locked loop is defined as the angular velocity multiplied by time, the deviation in phase is a linear function of time. Since it makes more sense to have phase angles in the interval $-\pi$ to π, the phase deviation signal is adjusted to achieve this before the signal is fed to the PI controller.

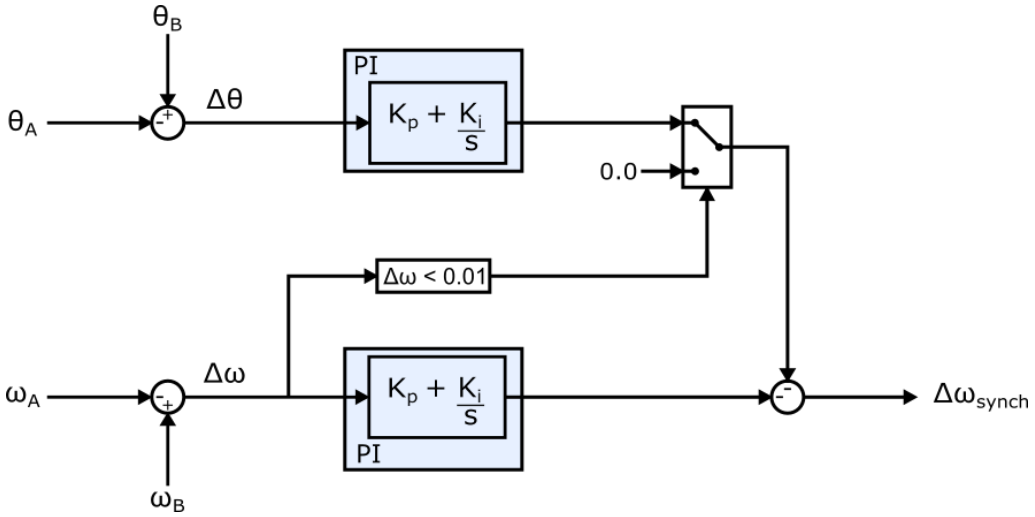

Figure 11: The proposed synchronization control loop. The control block diagram is adapted from [29].

5.3 Tuning of the synchronization loops

The PI controllers in the proposed synchronization control loops need to be given suitable gain values to achieve the desired system response. Before the gain values can be determined, a transfer function approximation of the microgrid system needs to be acquired.

5.3.1 Microgrid system approximation

To tune the PI controllers included in the proposed synchronization loops shown in Section 5.2.2, an approximation of the system is required. The synchronization loops affect only the smallest microgrid and it is thus necessary to find a system equivalent for this microgrid. The microgrid model is complex and it is therefore a difficult task to find the complete block diagram and the transfer function of the microgrid system. To find an approximation of the system transfer function, the system was perturbed by a step signal and the step response was recorded. This was accomplished by disconnecting the proposed synchronization loops and adding a step signal at the output of the synchronization loops. The step response of the microgrid system was recorded throughout the simulation.

The step response is shown as the red line in Figure 12, while the applied step signal is shown with the blue line. From the shape of the step response, the system is assumed to be of second order. A second order system transfer function can be described by the general form shown in Equation (37), where k is the DC gain, ζ is the damping ratio, and ω_n is the natural frequency [30].

$$H(s) = \frac{k\omega_n^2}{s^2 + 2\zeta\omega_n s + \omega_n^2} \tag{37}$$

From the system step response, the percentage of overshoot, OS, can be defined as in Equation (38), where f_{peak} is the peak value of the step response and f_{ss} is the steady state value of the step response.

$$OS = \frac{f_{peak} - f_{ss}}{f_{ss}} \tag{38}$$

The step response of the microgrid system has $f_{peak} = 0.2566$ and $f_{ss} = 0.2$. This results in $OS = 0.283$. From the percentage of overshoot, the damping ratio can be found through Equation (39). From this equation, the damping ratio of the microgrid system is found to be $\zeta = 0.3728$.

$$\zeta = \sqrt{\frac{(\ln(OS))^2}{\pi^2 + (\ln(OS))^2}} \tag{39}$$

The natural frequency, ω_n, can be found from the peak time, t_p, which is the time the step response uses to reach the peak value. From the peak time, the natural frequency is defined through Equation (40), and for the microgrid system it has a value of $\omega_n = 1.0041$.

$$\omega_n = \frac{\pi}{t_p\sqrt{1 - \zeta^2}} \tag{40}$$

Based on Equation (37), the values of $\zeta = 0.3728$ and $\omega_n = 1.0041$ found in Equations (39) and (40), and the DC gain of $k = 0.2$, the microgrid system to be synchronized with the proposed synchronization strategy can be expressed through the approximated transfer function in Equation (41). The step response of the approximate transfer function in Equation (41) is shown with a green line in Figure 12.

$$H_{sys}(s) = \frac{k\omega_n^2}{s^2 + 2\zeta\omega_n s + \omega_n^2} = \frac{0.2016}{s^2 + 0.7487s + 1.008} \tag{41}$$

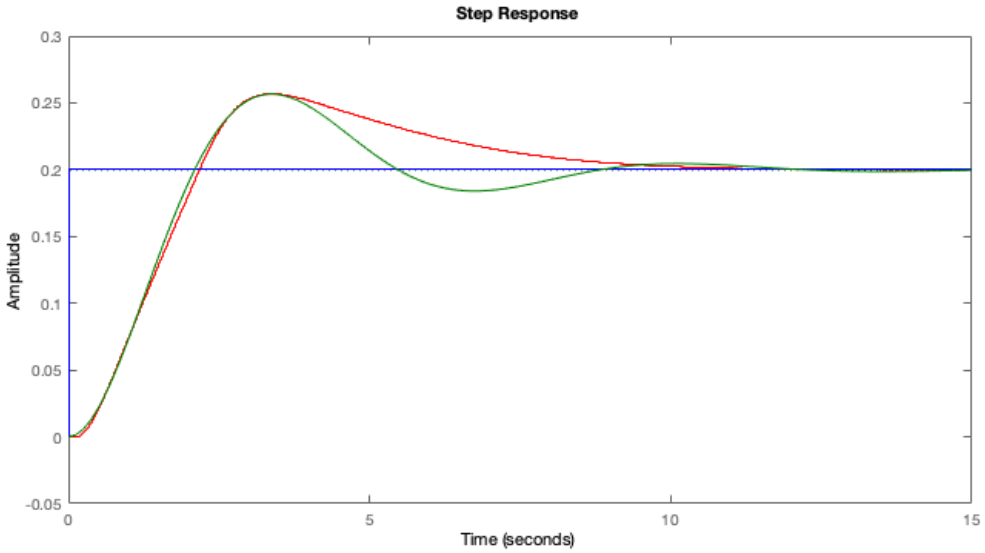

Figure 12: Step signal and step responses of the microgrid system and the approximated transfer function for the system.

By using the system approximation it is possible to find the transfer function of the synchronization control loops. To simplify the tuning process, the system approximation is reduced to a first order system. A first attempt of this was to find the first order equivalent approximation through imposing equal integrals of error, as was done to reduce the transfer function of the current control loop in Section 3.3.3. This approach is described in Equation (42), where ε_{sys} is the step response error of the second order system approximation, found in Equation (43), and $\varepsilon_{sys,EQ}$ is the step response error of the equivalent first order transfer function, found in Equation (44).

$$\int_0^\infty \varepsilon_{sys} dt = \int_0^\infty \varepsilon_{sys,EQ} dt \tag{42}$$

$$\varepsilon_{sys}(s) = \frac{k}{s} - \frac{k}{s} \frac{\omega_n^2}{s^2 + 2\zeta\omega_n s + \omega_n^2} \tag{43}$$

$$\varepsilon_{sysEQ}(s) = \frac{k}{s} - \frac{k}{s} \frac{1}{T_{eq}s + 1} \tag{44}$$

To find the integral from 0 to ∞ of the errors, the final value theorem for the Laplace transform, as described in Equation (45), is applied. The integrals of the errors are

calculated in Equations (46) and (47).

$$\lim_{t\to\infty} f(t) = \lim_{s\to 0} s \cdot F(s) \tag{45}$$

$$\lim_{t\to\infty} \int_0^\infty \varepsilon_{sys} dt = \lim_{s\to 0} \cdot s \frac{1}{s} \left(\frac{k}{s} - \frac{k}{s} \frac{\omega_n^2}{s^2 + 2\zeta\omega_n s + \omega_n^2} \right) = k \cdot \frac{2\zeta}{\omega_n} \tag{46}$$

$$\lim_{t\to\infty} \int_0^\infty \varepsilon_{sys} dt = \lim_{s\to 0} \cdot s \frac{1}{s} \left(\frac{k}{s} - \frac{k}{s} \frac{1}{T_{eq} s + 1} \right) = k \cdot T_{eq} \tag{47}$$

Inserting Equation (46) and (47) in Equation (42) results in the first order system equivalent shown in Equation (48) where the time constant is found to be $T_{eq} = \frac{2\zeta}{\omega_n}$. The step response of the first order system equivalent is shown as the red line in Figure 13.

$$H_{sys,EQ}(s) = \frac{k}{T_{eq} s + 1} = \frac{0.2}{0.7426 s + 1} \tag{48}$$

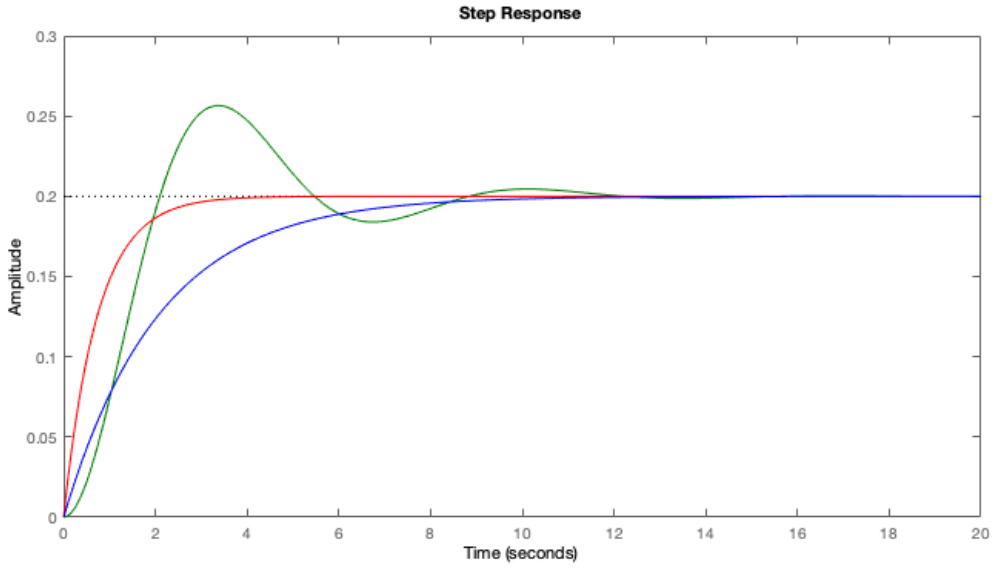

Figure 13: System approximation and two attempts of reduction from second to first order transfer function.

The first order equivalent found in Equation (48) is evaluated to have insufficient accuracy to proceed with. The next attempt at finding a first order equivalent takes instead the error squared and finds equal integrals of this, as shown in Equation (49).

$$\int_0^\infty \varepsilon_{sys}^2 dt = \int_0^\infty \varepsilon_{sys,EQ}^2 dt \tag{49}$$

Calculation of the error squared was performed with Wolfram Mathematica [31]. The inverse Laplace of Equation (43) and (44) was applied which result in Equation (50) and

(51).

$$\varepsilon_{sys}(t) = k \cdot e^{\zeta(-t)\omega_n} \left(\frac{\zeta \sinh\left(\sqrt{\zeta^2-1}\omega_n t\right)}{\sqrt{\zeta^2-1}} + \cosh\left(\sqrt{\zeta^2-1}\omega_n t\right) \right) \tag{50}$$

$$\varepsilon_{sysEQ}(t) = k - k\left(1 - e^{-\frac{t}{T_{eq}}}\right) \tag{51}$$

The square of the error was then found in the time domain and then transformed back to the Laplace domain, resulting in Equation (52) and (53).

$$\varepsilon_{sys}^2(s) = \frac{k^2\left(s^2 + 6\zeta\omega_n s + 2\left(4\zeta^2+1\right)\omega_n^2\right)}{\left(2\zeta\omega_n + s\right)\left(s^2 + 4\zeta s\omega_n + 4\omega_n^2\right)} \tag{52}$$

$$\varepsilon_{sysEQ}^2(s) = \frac{k^2}{s + \frac{2}{T_{eq}}} \tag{53}$$

To find the integral of the error squared, the Laplace function of the error was multiplied with $1/s$ and applied the final value theorem, as shown in Equation (54) and (55).

$$\lim_{t\to\infty} \int_0^\infty {\varepsilon_{sys}}^2 dt = \lim_{s\to 0} \cdot s \frac{1}{s} \left(\frac{k^2\left(s^2 + 6\zeta\omega_n s + 2\left(4\zeta^2+1\right)\omega_n^2\right)}{\left(2\zeta\omega_n + s\right)\left(s^2 + 4\zeta s\omega_n + 4\omega_n^2\right)} \right) = \frac{\left(4\zeta^2+1\right)k^2}{4\zeta\omega_n} \tag{54}$$

$$\lim_{t\to\infty} \int_0^\infty {\varepsilon_{sys}}^2 dt = \lim_{s\to 0} \cdot s \frac{1}{s} \left(\frac{k^2}{s + \frac{2}{T_{eq}}} \right) = \frac{k^2 T_{eq}}{2} \tag{55}$$

The first order equivalent with time constant of $T_{eq} = \frac{4\zeta^2+1}{2\zeta\omega_n}$ found from Equation (54) and (55) is shown in Equation (56). The step response of this first order approximation of the microgrid system is shown as the blue line in Figure 13.

$$H_{sys,EQ1}(s) = \frac{k}{T_{eq}s + 1} = \frac{0.2}{2.0783s + 1} \tag{56}$$

5.3.2 Tuning of the PI controllers

As the phase synchronization is not activated until the frequency deviation is smaller than 0.01, the PI controller of the frequency synchronization loop can be tuned individually from the phase synchronization PI controller. By looking at the frequency control loop only, the open loop transfer function of the frequency control loop is shown in Equation (57), where K_p is the proportional gain and T_i is the integral time constant of the PI controller. The last fraction in the expression is the first order equivalent of the microgrid system with DC gain $k = 0.2$ and time constant $T_{eq} = 2.0783$.

$$H_{OL,\omega}(s) = K_p \frac{1 + T_i s}{T_i s} \frac{k}{T_{eq}s + 1} \tag{57}$$

Based on the transfer function in Equation (57), the PI controller time constant is chosen to achieve pole-cancellation. This is realized by imposing $T_i = T_{eq}$. The pole cancellation reduces the transfer function to Equation (58).

$$H_{OL,\omega}(s) = \frac{K_p \cdot k}{T_{eq} s} \tag{58}$$

The proportional gain, K_p, is then chosen by imposing the crossover frequency. The crossover frequency, $\omega_{c\omega}$, is defined as the frequency where the magnitude of the transfer function is equal to 1. The value of K_p is defined as shown in Equation (59). The crossover frequency is set to $\omega_{c\omega} = 0.16$ which results in $K_p = 1.6626$. From K_p and T_i, the integral gain of the PI controller is calculated to be $K_i = K_p/T_i = 0.8$. The closed-loop transfer function of the frequency controller is shown in Equation (60). This tuning, when tested, showed satisfactory results.

$$|H_{OL,\omega}(j\omega_{c\omega})| = \left| \frac{K_p \cdot k}{T_{eq} \cdot j\omega_{c\omega}} \right| = 1 \longrightarrow K_p = \frac{\omega_{c\omega} \cdot T_{eq}}{k} \tag{59}$$

$$H_{CL,\omega}(s) = \frac{H_{OL,\omega}}{1 + H_{OL,\omega}} = \frac{1}{\frac{1}{\omega_{c\omega}} s + 1} \tag{60}$$

When it comes to tuning of the phase synchronization loop, the proposed parallel configuration of the frequency and phase PI controllers complicates the tuning process. Thus, and alternative series cascaded configuration of the PI controllers, as seen in [27], was studied. With this configuration, the phase synchronization loop acts as an outer control loop. The open-loop transfer function of the phase synchronization loop can thus be expressed as in Equation (61), where K_p is the proportional gain and T_i is the integral time constant of the PI controller. The second fraction is the closed-loop transfer function of the inner loop, and the last fraction is the integration from frequency to phase angle. The frequency is in pu so to find the phase angle it is necessary to scale it with the base value $\omega_{base} = 2\pi \cdot 50$ rad/s.

$$H_{OL,\theta}(s) = K_P \frac{1 + T_i s}{T_i s} \cdot \frac{1}{\frac{1}{\omega_{c\omega}} s + 1} \cdot \frac{\omega_{base}}{s} \tag{61}$$

Since the transfer function of the phase controller has a double pole at the origin, symmetrical optimum is applied to tune the PI controller. The time constant of the PI controller T_i is assumed to be larger than the time constant of the inner control closed-loop transfer function and is thus defined as $T_i = \frac{a^2}{\omega_{c\omega}}$. For symmetrical optimum, crossover frequency, $\omega_{c\theta}$, should be imposed at maximum phase which occurs at $\omega_{c\theta} = \frac{\omega_{c\omega}}{a}$. This results in Equation (62).

$$\begin{aligned} |H_{OL,\theta}(j\omega_{c\theta})| = \left| -K_p \omega_{base} \frac{1}{\frac{a^2}{\omega_{c\omega}} \frac{\omega_{c\omega}}{a}^2} \cdot \frac{1 + \frac{a^2}{\omega_{c\omega}} \cdot j\frac{\omega_{c\omega}}{a}}{1 + \frac{1}{\omega_{c\omega}} \cdot j\frac{\omega_{c\omega}}{a}} \right| = K_p \cdot \frac{\omega_{base}}{\omega_{c\omega}} \cdot a = 1 \\ \longrightarrow \quad K_p = \frac{\omega_{c\omega}}{a \cdot \omega_{base}} \end{aligned} \tag{62}$$

With these tuning parameters applied to the microgrid system, the results are not satisfactory as the microgrid does not reach synchronization. As tuning through theoretical

calculations did not achieve satisfactory results in this case, the PI controller in the phase synchronization loop was tuned through trial and error, with the initially thought parallel configuration shown in Section 5.2.2. Through trial and error, the proportional gain, $K_p = 0.007$, and integral gain, $K_i = 0.006$, of the PI controller in the phase synchronization loop was determined.

6 Description of the simulation model

The synchronization control strategy described in Section 5.2.2 is tested in simulations to verify that it achieves the requirements of synchronization. The simulation model consists of two simplified microgrids that are connected through a switch. The simulation time is set to 30 seconds, where the switch connecting the two microgrids is closed 25 seconds into the simulation. The simulation does not address steady state operation of the grids in neither islanded or grid-connected operation, but is limited to look at the synchronization process and the immediate conditions in the interconnected grids after the switch closes.

The simulation model of a single microgrid used in this thesis is provided by SINTEF Energy from the project "MultiGrid", which this thesis is related to. The parameters used in the thesis for the converter unit, the synchronous generator system and the transformer where already included in the model before used in this thesis. The model of the microgrid from SINTEF was used to compose the multigrid model, consisting of two microgrids that are to interconnect. The synchronization technique proposed in this thesis was added.

6.1 System overview

The simulation model is schematically presented in Figure 14. The figure shows two microgrid areas, Microgrid A and Microgrid B, connecting through a switch. Both of the modeled microgrids have two sources of power that together supply a common local load. The two power sources in the microgrids are a synchronous generator, with a gas turbine prime mover, and a converter-based generating unit. The source of power on the DC-side of the converter is not specified and is, for simplicity, modeled as a constant current source. The two microgrids have the same components but Microgrid B is given a slightly higher power rating of the synchronous generator and a higher load.

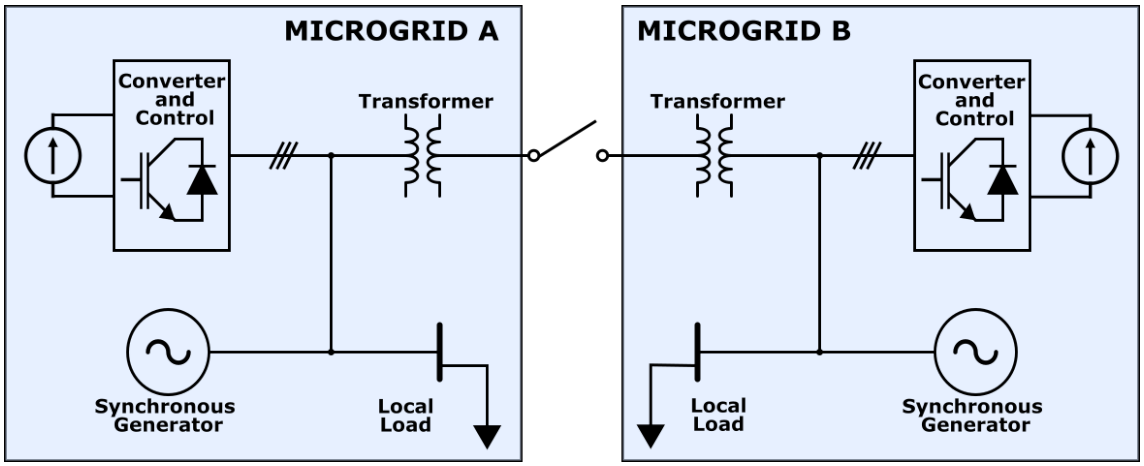

Figure 14: Schematic of the multigrid simulation model.

Each microgrid has a rated three-phase alternating voltage of 400 V (line-line) and a nominal frequency of 50 Hz. In both microgrids, the voltage is transformed up to 20 kV before it reaches the connection switch. The microgrid systems have rated power of 50 kVA. The rated values of the two microgrids are summarized in Table 1.

Table 1: Rated values of Microgrid A and B

Parameter	Symbol	Value
Nominal line voltage	V_n	400 V
Nominal frequency	f_n	50 Hz
Rated apparent power	S_n	50 kVA

The proposed synchronization technique is implemented in the multigrid model. Voltage measurement signals are sent from each side of the connection switch to the microgrid central controller, where the synchronization control loops are located. The control loops provide an angular frequency offset signal. The offset signal is added to the speed reference of the synchronous generator in Microgrid A. The parameters of the synchronization control loops are presented in Table 2.

Table 2: Parameter values of the synchronization control loops.

Parameter	Symbol	Value
Proportional gain PLLs	$K_{p,PLL}$	5.3052
Integral gain PLLs	$K_{i,PLL}$	58.9463
Proportional gain frequency controller	$K_{p,\omega}$	1.6626
Integral gain frequency controller	$K_{p,\omega}$	0.8
Proportional gain phase angle controller	$K_{p,\theta}$	0.007
Integral gain frequency PI controller	$K_{p,\theta}$	0.006

Each of the components in the two microgrids, the voltage source converter, the synchronous generator system and the local load, are now in turn explained and their sizing and control parameters are determined.

6.2 Voltage Source Converter

The voltage source converter system, which is connected to the microgrid as a power source, is schematically shown in Figure 15. The DC-side voltage of the converter is supplied by a constant current source, representing a renewable energy source, such as solar PV power. The converter transforms power from a direct voltage with 700 V amplitude to a three-phase alternating voltage of 400 V (line-line) amplitude with nominal frequency of 50 Hz. The converter has rated value for the current at 50 A, and a rated power of 34.641 kVA. The switches in the converter have a switching frequency of 5 kHz.

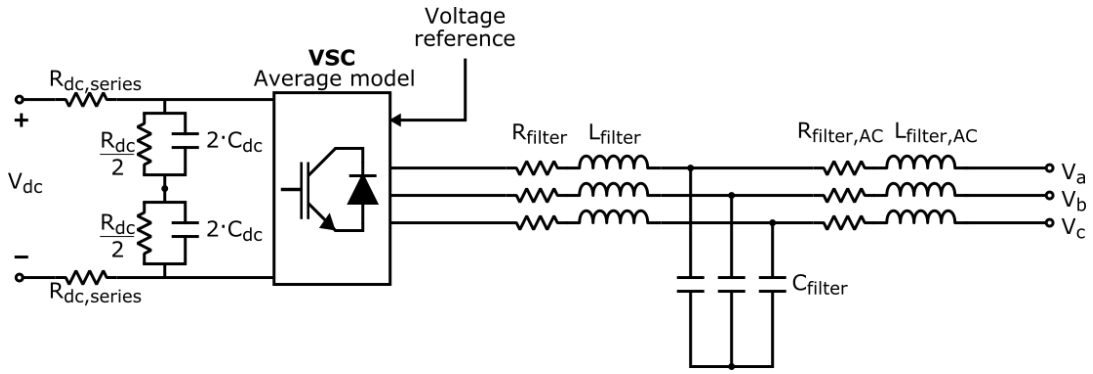

Figure 15: Circuit diagram of the voltage source converter interfacing the microgrids.

Due to the switching characteristics of voltage source converters, the output voltage at the converter terminals contains high order harmonics. Thus, an LCL-filter is applied at the output terminals of the converter to provide the grid with a more refined alternating voltage. The LCL-filter of the converter is shown in Figure 15, at the output terminals of the converter. The series resistances R_{filter} and $R_{filter,AC}$ are the inductor resistances of inductors L_{filter} and $L_{filter,AC}$. Between the two inductors, the filter contains a capacitor C_{filter} connected to ground. At the DC-side of the converter there are resistances and capacitances in parallel with the current source at the converter DC terminals. In addition, a series resistance is included between the DC terminals of the converter and the parallel resistances and capacitances.

As the design of the converter and all parameters are adapted from the model received by SINTEF, the circuit component values are presented in Table 3 without further explanations, along with rated values of the converter.

Table 3: Rated values and circuit parameters of the voltage source converter.

Parameter	Symbol	Value
Nominal line voltage	V_n	400 V
Nominal current	I_n	50 A
Nominal frequency	f_n	50 Hz
LCL-filter values:	R_{filter}	46.2 mΩ
	L_{filter}	1.5 mH
	$R_{filter,AC}$	46.2 mΩ
	$L_{filter,AC}$	1.5 mH
	C_{filter}	55.133 μF
DC side circuit parameters:	R_{DC}	19.707 kΩ
	C_{DC}	2.8 mF
	$R_{DC,series}$	49.3 kΩ

6.2.1 Parameter values for the voltage source converter control

The parameter values for the control loops of the voltage source converters are given in Table 4. The gain values of the PLL and current controller are found from the equations derived in Section 3.3.2 and Section 3.3.3, respectively. However, for the DC voltage controller, the theoretical tuning technique derived in Section 3.3.4 does not give acceptable results. This is due to the fact that the theoretical tuning technique is based on a single capacitor at the DC side terminals of the converter. In the converter model used for the simulations in this thesis, the DC side of the converter also includes series and parallel resistances, which have influence on the performance of the controller. The gain values used for the DC controller are provided along with the model from SINTEF.

Table 4: Parameter values for the control loops of the voltage source converter

Parameter	Symbol	Value
Proportional gain current controller	K_{pc}	1.3263
Integral gain in current controller	K_{ic}	41.6667
Proportional gain DC voltage controller	K_{pv}	4
Integral gain in DC voltage controller	K_{iv}	200
Proportional gain PLL	$K_{p,PLL}$	5.3052
Integral gain PLL	$K_{i,PLL}$	58.9463
Symmetrical optimum tuning coefficient	a	3
DC-voltage reference	$V_{dc,ref}$	700

6.3 Synchronous generator

The synchronous generator systems are modeled with a gas turbine model as the prime mover. The synchronous generator supplies the microgrids with an alternating voltage of amplitude 400 V, with a frequency of 50 Hz. The synchronous generators in the two microgrids are of similar size, but the synchronous generator of Microgrid B is chosen to be 12% higher than the synchronous generator of Microgrid A. The rated power of the synchronous generators are 62.5 kVA and 70 kVA, respectively. The rated values of the synchronous generators in the two microgrids are summarized in Table 5.

Table 5: Rated values of the synchronous generator system in Microgrid (MG) A and B.

Parameters	Symbol	Value
Nominal voltage	V_n	400 V
Nominal frequency	f_n	50 Hz
Rated apparent power	S_n	62.5 kVA (MG A)
		70 kVA (MG B)

The generator system includes an excitation system which provide the field voltage to be

applied to the rotor. The parameter values of the excitation system, and the parameters of the synchronous generator are presented in Appendix A.

6.3.1 Parameter values for the synchronous generator governor model

The governor systems for these synchronous generators, modeled as gas turbines governors, are presented in Section 4.2. All the control parameters used in this thesis were included in the model of the synchronous generator system provided by SINTEF. These values are presented in Table 6.

Table 6: Parameter values of the synchronous generator governor model.

Parameters	Symbol	Value
Turbine lag time constant	T_b	0.1 s
Turbine gain	K_{turb}	1.873
No load fuel flow	w_{nlf}	0.17 pu
Max fuel valve opening	V_{max}	0.704 pu
Min fuel valve opening	V_{min}	0.09 pu
Max rate of increase fuel command	$rateOpen$	3.3 pu/s
Min rate of increase fuel command	$rateClose$	-3.3 pu/s
Fuel flow actuator time constant	T_{act}	0.2 s
Governor proportional gain	K_{pgov}	5.5
Governor integral gain	K_{igov}	2
Governor derivative gain	K_{dgov}	1
Time constant for derivative gain	T_{dgov}	1 s

6.4 Local load

The demand of each microgrid is modeled as one common local load, connected to the two power sources. The load in each microgrid is assumed to be inductive and draws power from the grid based on the applied voltage. The load demand of the two microgrids are slightly different in size, where the load demand is 12% higher in Microgrid B. For the reference scenario the load demand is at $31.25 + j6.25$ kVA in Microgrid A and at $35.0 + j7.0$ kVA in Microgrid B.

7 Results

The proposed synchronization technique, described in Section 5.2, is tested through simulations to verify that the synchronization loops fulfill the task of synchronizing the microgrids upon connection. The technique is tested under different conditions in several simulations to challenge the robustness of the synchronization loop.

Circuit parameters and rated values of the model used in the simulations are presented in Section 6. The model consists of two simple microgrid models, Microgrid A and Microgrid B, connecting through a circuit breaker switch. For all simulations the switch closes at 25 seconds. The synchronization process starts 0.6 seconds into the simulation, after all loads and generating units, as well as their control loops, are enabled. The synchronization loops are designed to synchronize Microgrid A to match the operating conditions of Microgrid B. The simulations performed are thus focused on Microgrid A, since this grid is directly affected by the proposed synchronization technique. Throughout all simulations, the conditions of Microgrid B are kept static while variations to operating conditions are applied to the smaller microgrid, Microgrid A.

Microgrid B is throughout all simulations supported by generation from both the synchronous generator and the converter-based generating unit. The converter unit is connected to a current source that supplies a current of 35 A. The remaining power demand is met by the synchronous generator. The local load of microgrid B has a power demand of $35 + j7$ kVA. The speed reference for the generator governor is 1 pu with a base value of $2\pi f_n$, where f_n is the nominal frequency of 50 Hz.

7.1 Reference scenario

A reference scenario of operating conditions in Microgrid A is used for the simulations. In this scenario, the local load has a power demand of $31.25 + j6.25$ kVA. The load is supported by generation from both the converter-based generating unit and the synchronous generator. The converter unit has a current source that provides a current of 31.25 A. The synchronous generator covers the remaining load demand. Since both microgrids are designed to follow the nominal frequency, f_n, the speed reference of the synchronous machine governor is adjusted to force a frequency deviation between the two grids. For the reference scenario this speed reference is set to 0.9 pu, which translates to a 10% lower frequency than in Microgrid B.

If no synchronization is applied to the microgrids before they are interconnected, large inrush currents arise at the moment of connection. To verify this, the model is run through a simulation where the synchronization loops are deactivated. The angular frequency and phase angle deviations throughout the simulation are shown in Figure 16. The currents at the terminals of the grid components in Microgrid A and at the interconnection point between the two grids are shown in Figure 17.

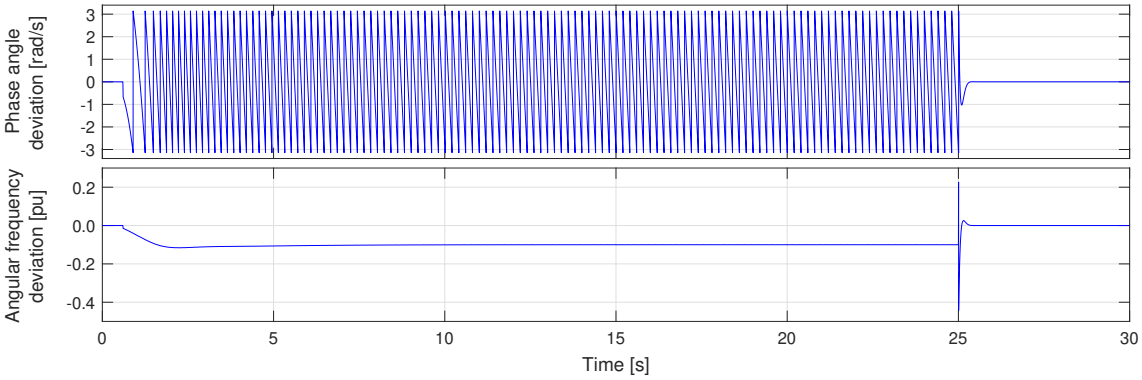

Figure 16: Deviations in phase angle and angular frequency between the two microgrids when no synchronization is applied.

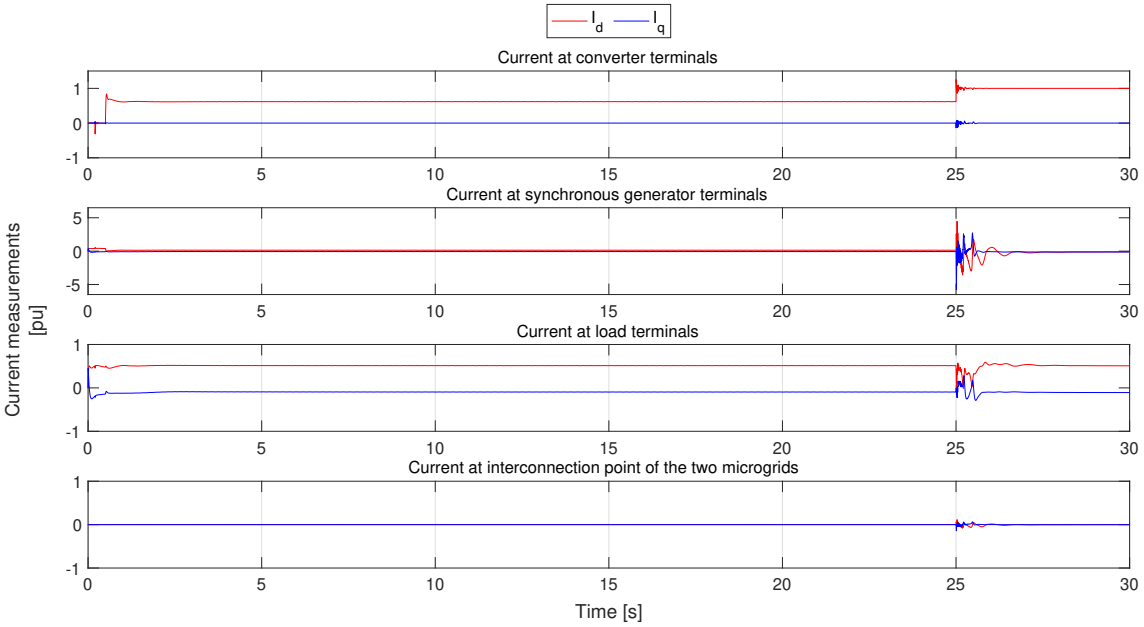

Figure 17: The d- and q-components of the current at the component terminals within Microgrid A and at the point of common coupling.

From the deviation plots in Figure 16, it can be seen that there are deviations in both angular frequency and phase angle at the interconnection moment. As the angular frequency deviation in the lower plot is in per unit values, this deviation will directly translate to the per unit deviation in frequency between the two microgrids. The upper plot shows the phase angle deviation between the two grids. At the time of interconnection the phase angles in the two grids deviate significantly. This results in spikes in both angular frequency and phase angle deviations directly after the switch closes and connects the two grids. The spikes are a result of the system canceling out the deviations between the two grids.

The angular frequency deviation will stabilize at a certain value. This value is different from 0 since the speed reference for the two grids are chosen to be different to force a frequency deviation between the two grids. The problem with a deviation in frequency between the two grids is well illustrated in Figure 16. The frequency deviation will cause the phase deviation to continuously change as a result of Microgrid B being faster than Microgrid A.

From the plots of the currents in Microgrid A in Figure 17, it is possible to see the effect on the currents when the two microgrids interconnect without being synchronized. The current measurements are collected at the terminals of the converter-based generating unit, the terminals of the synchronous generator, the load terminals and at the interconnection point between the two microgrids. The plots show the d- and q- components of the currents, where the red lines represents the d-component and the blue lines represents the q-component. The current measurement values are given in per unit value. However, the base values are not equal for all the current measurements. The base values for the converter and synchronous generator current are the rated current for the two units, respectively. The base value for the load current and the current at the interconnection point is the rated current of the system.

The most severe occurrence of high inrush currents is at the synchronous machine terminals. Here the currents have oscillations that reach an amplitude of as much as -5 and 5

pu. The current at the converter terminals have a rise in the current that exceeds 1 pu, but not to the same extent as at the synchronous generator terminals. The load will also experience the effect of the out of phase and frequency reclosing of the switch significantly. It is thus evident that synchronizing actions are needed before the two microgrids can be interconnected.

The proposed synchronization technique is now activated and the simulation is run again. The result of this simulation is presented in Figure 18, and shows the deviations in phase angle and angular frequency. Figure 19 shows the current measurements in Microgrid A.

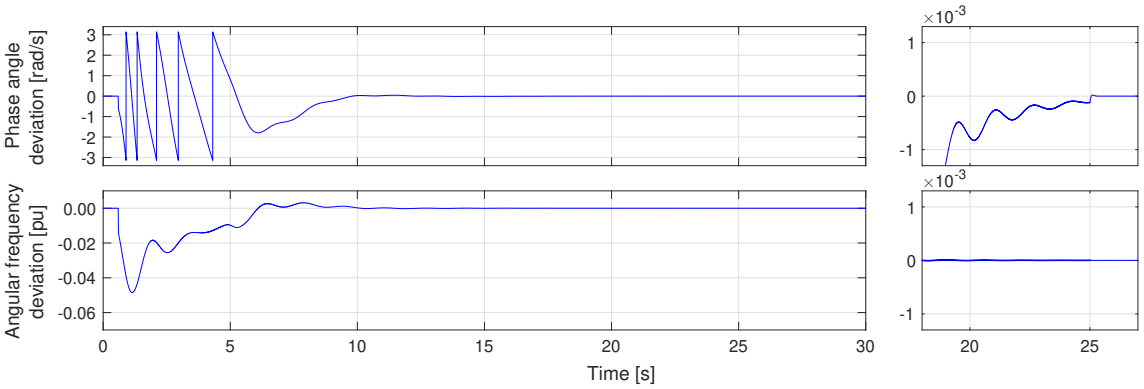

Figure 18: Deviations in phase angle and angular frequency between the two microgrids when the synchronization loops are activated.

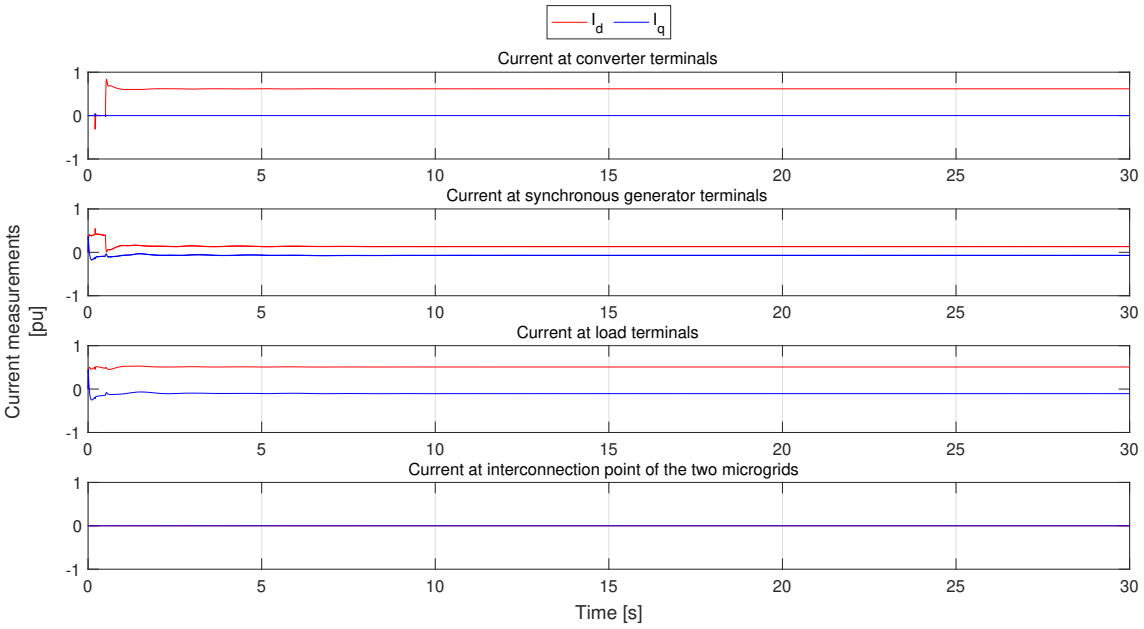

Figure 19: The d- and q-components of the current at the component terminals within Microgrid A and at the point of common coupling.

In Figure 18, it can be seen that the synchronization loops successfully eliminate the deviations in angular frequency and phase angle within the allowable limits. The figure shows four plots. The upper two plots show the deviation in phase angle. The left plot show the phase angle deviation throughout the whole simulation period, with the full range of phase angle errors. The right plot shows a more detailed view of the phase angle

deviation around the time of interconnection at 25 seconds. The deviation amplitude axes is zoomed in and is chosen to range from -0.001 to 0.001. The reason for this is that these values are the lower and upper threshold values for synchronization, chosen for this thesis. The lower two plots show the angular frequency deviation. Also here, the left plot shows the deviation in full range for the whole simulation period. The right plot provides a more detailed view around the time of interconnection with axis limits equal to the lower and upper threshold values for synchronization.

The thresholds for allowable deviations were defined in Section 5.2 to be 0.001 pu for the angular frequency and 0.001 rad/s for the phase angle. Both of the detailed plots to the right in Figure 18 show that the deviations are well within these values when the switch close. It can also be seen that there are no spikes in the deviation graphs at the point of interconnection, as could be seen in Figure 16.

The synchronization technique is designed so that the elimination of the phase angle deviation is not activated before the frequency deviation is sufficiently small. This can be seen in Figure 18. In the figure, the following observations can be made:

1. Only the frequency PI controller loop is active the first ~ 5 seconds.
2. About 5 seconds into the simulation, the frequency deviation reaches a deviation with absolute value lower than 0.01.
3. The phase angle PI controller loop is activated and the phase angle deviation starts trending towards zero.

In addition to the phase synchronization being activated later than the frequency synchronization, the elimination time of the phase deviation is much larger than that of the frequency deviation. The reason for this is that the phase deviation is much larger in size as it can vary between $-\pi$ and π in magnitude. Since the frequency deviation is expressed in per unit value, this value will be much smaller than that of the phase deviation value. Thus, the frequency deviation will reach synchronization faster.

The effect of the synchronization on the currents in Microgrid A is presented in Figure 19. The figure shows four plots of current measurements at different locations within Microgrid A, presented in the dq-frame components. Contrary to Figure 17, there are no visible current transients that arise when the two microgrids interconnect.

Thus, it can be stated that the synchronization loops successfully eliminate the risk of high inrush current transients in the microgrids. However, since the conditions in the model are very case specific, the robustness of the synchronization loops is tested by running additional simulations where the operating conditions in Microgrid A are slightly altered. This is done by changing one parameter multiple times while keeping all other parameters at the operating conditions value defined for the reference scenario.

7.2 Varying the frequency deviation

As the individual frequencies of the two microgrids are a result of the balance between intermittent load and generation, the frequencies of the two grids might deviate from each other. Thus, the synchronization loops need to be robust enough to manage synchronizing the microgrids with varying deviations in frequency. The microgrid models include speed control of the synchronous generators. These have originally a speed reference of 1 pu,

where the base value for the rotational speed is 2π times the nominal frequency of 50 Hz, $\omega_{base} = 2\pi f_n$.

To force frequency deviations between the two microgrids, the speed reference of the synchronous generator of Microgrid A is changed. In the reference scenario, the speed reference for the synchronous generator in Microgrid A is set to 0.9 pu. To check the robustness of the synchronization loops when it comes to frequency deviation, additional simulations are performed with speed references 0.7, 1.0 and 1.1 pu. All other parameters are kept equal to those of the reference scenario.

The collected results from the simulations are presented in Figure 20. Additionally, the simulation result of the reference scenario is added as the black line in the figure. The layout of the figure is the same as in Figure 18. The upper two plots show the phase angle deviation for the whole simulation period and a more detailed view around the interconnecting point, and the two lower plot show the same views of the angular frequency deviation.

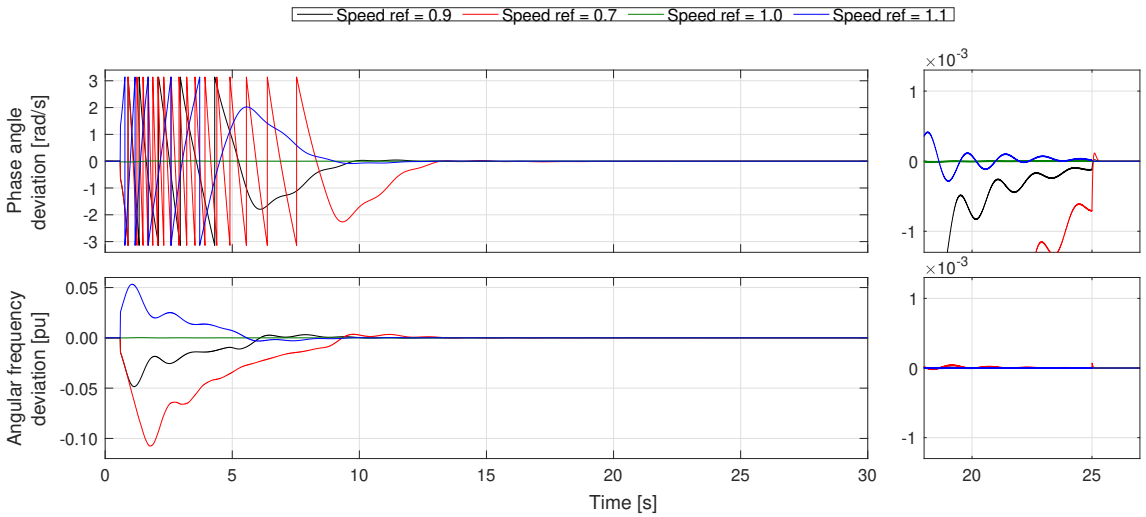

Figure 20: Deviations in phase angle and angular frequency between the two microgrids for different speed reference values.

For the tested values of speed references, the synchronization loops manage to sufficiently eliminate the deviations in both phase angle and angular frequency. Both of the deviations are within the threshold values, defining the microgrids as synchronized, before the switch closes and the microgrids are connected.

The larger the frequency deviation forced upon the two microgrids is, the longer it takes before the phase angle synchronization loop is activated. The reason for this is that the phase angle synchronization loop is not activated before the angular frequency deviation is less than ± 0.01. For the reference scenario, as well as the scenario with speed reference 1.1, the synchronization loop for the phase angle deviation is activated after ~ 5 second into the simulation.

With speed reference equal to 0.7, and thus a much larger initial frequency deviation between the two grids, it takes longer before the frequency deviation is smaller than 0.01. Thus, the synchronization loop for the phase angle deviation does not take part in the synchronization process before it has passed ~ 8 seconds. The synchronization of the phase angle is shifted in time relative to the reference scenario. Thus, the phase deviation

is larger than that of the reference scenario when the switch closes. With the speed reference of Microgrid A set to 0.7, the speed reference deviation between the two grids are 0.3 pu. This represents a large frequency deviation. It might not be realistic to look at deviations of this size as the microgrids will attempt to maintain the rated frequency, also in islanded operation.

In order to to verify that the synchronization loops also work when there initially are no deviation in frequency, a simulation is conducted with no speed reference deviation between the two grids. The deviations in phase angle and angular frequency are so small that they are not shown in Figure 20. An interesting situation to test through simulations would be to see how the synchronization loops would react if the phase angle deviation was of great significance while there was no significant frequency deviation between the two grids. This was, however, not tested in this thesis work.

7.3 Variation in share of power production from the converter unit

The microgrid under synchronization during the simulation, Microgrid A, consists of both power generation from a synchronous generator and from a converter-based unit. This means that there are both generation from a unit that provides inertia to the system and from a unit that does not. In microgrids, the presence of renewable sources is common, and is usually the source of power connected to the DC side of voltage source converters. As generation from renewable energy sources are intermittent, it is relevant to look into the robustness of the synchronization loops when the share of power production from the converter unit increase and decrease with respect to the reference scenario.

In the reference scenario the current source on the DC side of the converter in Microgrid A supplies a current of 31.25 A. To check the robustness of the synchronization technique with different share of power production from the converter-based unit, simulations are conducted where the supply of current from the current source varied. The size of the current source, connected to the DC side of the converter, are set to 0, 10 and 40 A. All other values are kept equal to those in the reference scenario. The results of the simulations are shown in Figure 21. The two upper plots show the phase angle deviations and the two lower plots show the angular frequency deviations during the simulations.

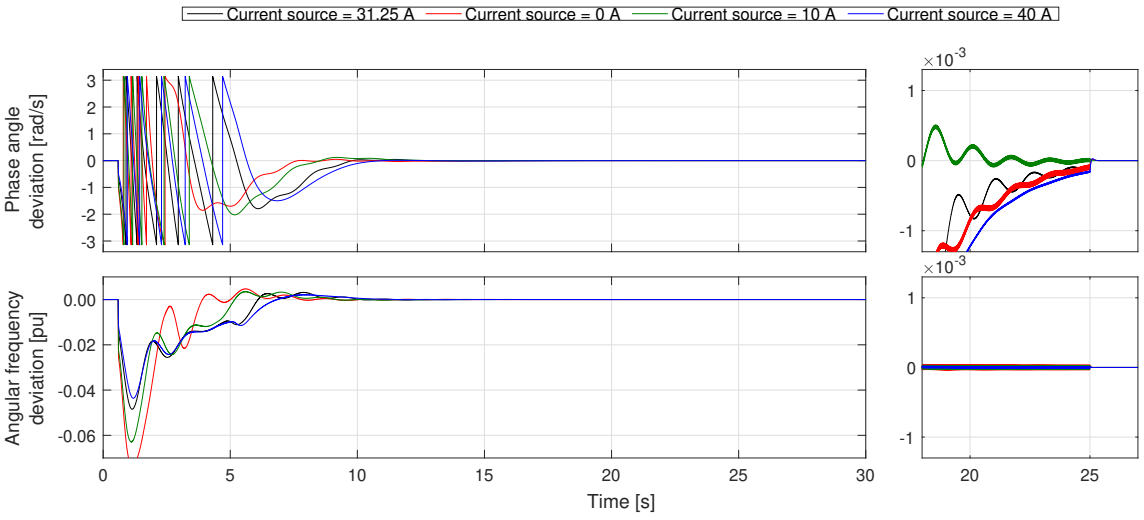

Figure 21: Deviations in phase angle and angular frequency between the two microgrids for different current values from the converter DC side current source.

As seen in the lower plot of Figure 21, decreasing the share of power production from the converter-based unit will result in larger overshoot in the frequency deviation at the beginning of the synchronization process. The frequency deviation curve for a current source of 0 A, shown as the red line, have a negative peak of less than -0.06 pu while the cases with larger current sources, such as 31.25 and 40 A, have a negative peak above -0.05 pu.

Looking closely at the upper plot in Figure 21, the phase angle deviation lines representing higher converter current source values will start to synchronize later. However, it is the green line, representing a current source of 10 A, that has the biggest overshoot and is the fastest to synchronize within the threshold values. Thus, there is no linear relation between the size of the current source and how fast the phase angle deviation is eliminated.

7.4 Varying the inertia constant of the synchronous generator

The model of the synchronous generator used in the simulation model is a copy of a generator model meant for larger generating units. The base values for the system is altered to fit the model to present a smaller synchronous generator, which is more likely to be included in a microgrid configuration. It is thus assumed, in the reference scenario, that the per unit parameters in the model of a large power plant is accurate also for a smaller unit. However, some per unit parameters in a smaller unit, like the inertia constant, might differ from the per unit parameters of a large synchronous machine power plant.

The robustness of the synchronization loops is thus tested for different values of the inertia constant of the synchronous generator in Microgrid A. Simulations are conducted for inertia constant values of 2 and 6 seconds. The values are chosen to see the effect on the synchronization process for a slightly smaller and larger value of the inertia constant than in the reference scenario. The results are shown in Figure 22. The two upper plots show the phase angle deviation and the two lower plots show the angular frequency deviation of Microgrid A during the simulations.

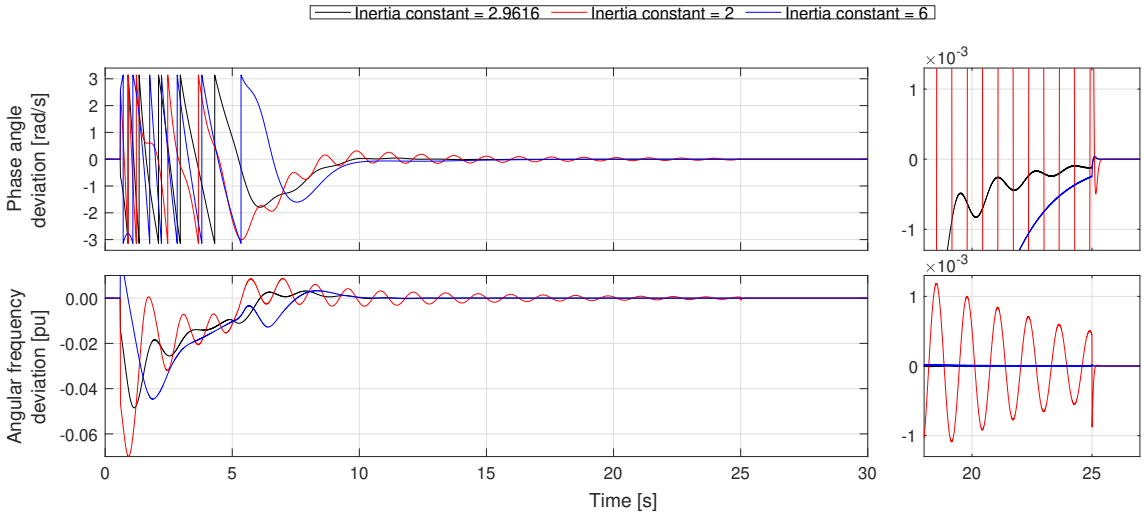

Figure 22: Deviations in phase angle and angular frequency between the two microgrids for different inertia constant values.

From Figure 22 it can be seen that for the lower inertia constant value of 2 seconds, the proposed synchronization loops do not fulfill the synchronization criteria within 25 seconds. With lower inertia the deviation graphs oscillate significantly more than in the reference scenario, and the responses of the loops tend towards unstable. With an even smaller inertia constant it can be assumed that the responses of the synchronization loops will reach instability. The occurrence of the oscillations might be a result of too high PI controller gains as the tuning is not based on the smaller inertia value. However, the inertia constant of a single machine is constant, which means that the synchronization loops for a generator will be tuned to match the characteristics of the machine.

The simulation with a higher value for the inertia constant, $H = 6$ seconds, shows that the synchronization loops successfully manage to synchronize the microgrid within the decided allowable values of deviation. However, the synchronization process is slower than in the reference scenario, and the synchronization of the phase angle is thus activated later than in the reference scenario. Although the synchronization is a bit slower with the higher inertia constant, the responses of the synchronization loops are smoother and less subject to oscillations.

From the simulations with various inertia constants of the synchronous machine that takes part in the synchronization process, it can be noted that the inertia constant has a large effect on the synchronization process.

7.5 Variations in load

The microgrid to be synchronized needs to supply the local load, also during the synchronization process. The load is not specified in the model and a real microgrid will include several loads. It may vary when the different loads are in need of power. Thus, the total load demand in the microgrid might vary during normal operation. This applies to the size of the load demand, but also how resitive or inductive the total combined load is. For this reason, the proposed synchronization technique is tested for various load conditions in Microgrid A. Simulations are performed with both static and dynamic load variations.

7.5.1 Static load variation

First, simulations on static load variations are performed. With static load variations it means that the load does not change during the simulation period. The load variations are applied between each simulation. In the reference scenario the microgrid supply a load of $31.25 + j6.25$ kVA. The synchronization loops are also tested with the microgrid supporting a purely resistive load of 31.25 kW, and supporting a more inductive load of $31.25 + j25$ kVA. The results are shown in Figure 23. Also here, the upper two plots show the phase angle deviation while the lower two plots show the angular frequency deviation.

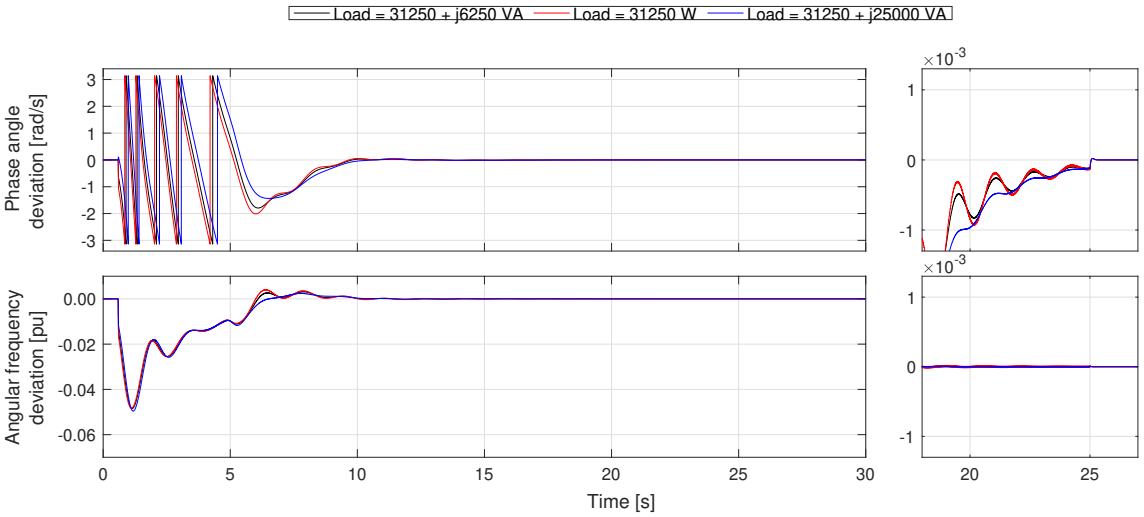

Figure 23: Deviations in phase angle and angular frequency between the two microgrids for different load values.

Figure 23 shows that the synchronization technique works for both resistive and inductive loads. The synchronization time of the three simulations with varying load is approximately the same. The more inductive the local load in the microgrid is relative to resistive, the less oscillations can be seen in the responses of the synchronization loops.

7.5.2 Dynamic load variation

In reality, a microgrid will not only supply power to a single local load, but to a multiple of different loads in near geographical proximity. The variety of loads in the microgrid might not always have the same load demand. The load demand in a microgrid can be intermittent and unreliable. Load variations may thus occur in the period where the microgrid undergoes the synchronization process. Therefore, simulations are conducted to check the robustness of the proposed synchronization technique when a change in the load demand happened during the synchronization process.

Simulations were performed for both an increase and a decrease in the load demand. The load variation that occur during the simulation process is chosen to be in the size of 5% of the reference scenario load demand. This amounts to an increase and a decrease of approximately $1.56 + j0.31$ kVA. Different simulations are performed to check if the synchronization loops could withstand a load variation at different times in the synchronization process. The load variation is added and subtracted from the local load in the microgrid model at 5, 10 and 15 seconds into the simulation. The results of the load increases are shown in Figure 24, and the results of the load decreases are shown in Figure 25. In both figures, the upper plots show phase angle deviations and the lower plots show the angular frequency deviation between the two interconnecting microgrids.

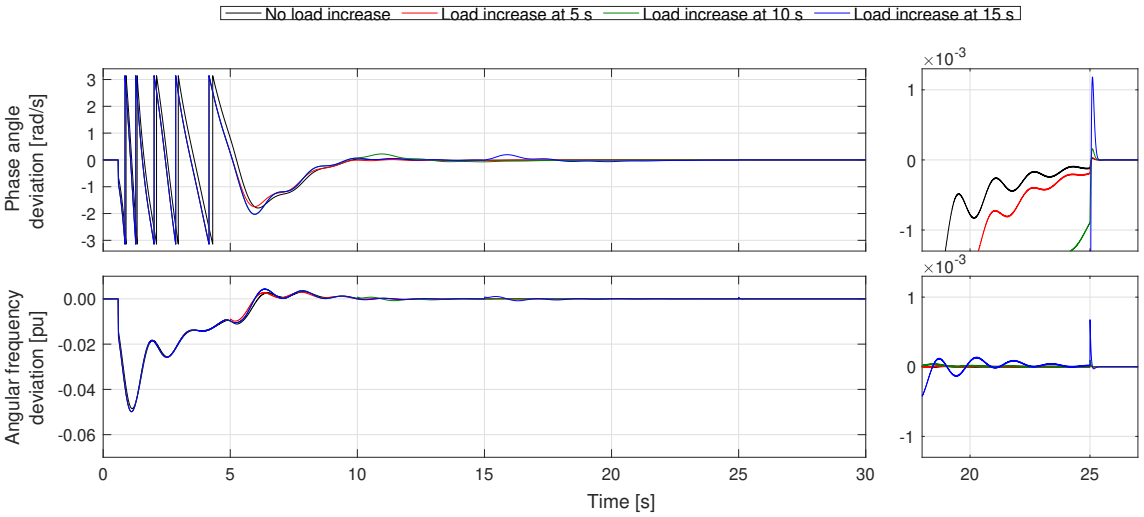

Figure 24: Deviations in phase angle and angular frequency between the two microgrids for a 5% load increase at different moments during the simulation.

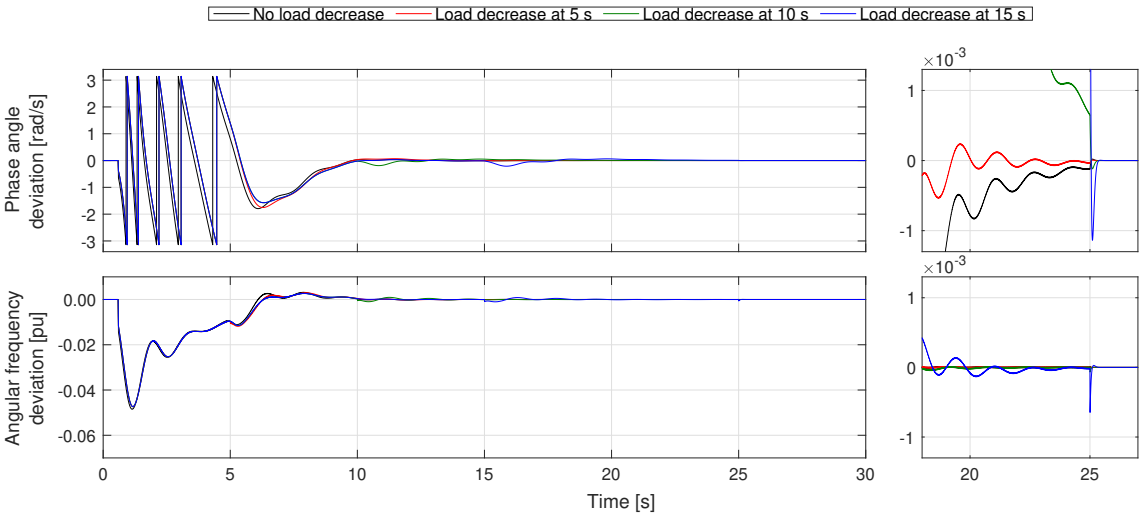

Figure 25: Deviations in phase angle and angular frequency between the two microgrids for a 5% load decrease at different moments during the simulation.

When load variations happen during the synchronization process, it makes the process of reaching synchronization within the allowable deviation limits slower. The closer the deviations are to synchronization when the load variation happen, the longer the synchronization process needs to be. This is illustrated in the upper right plot in Figure 24 and 25. The green and blue lines, representing load variations at 10 and 15 seconds into the simulation, have not yet reached the same synchronization as the other two simulations when the switch closes at 25 seconds.

The load changes influence the phase deviation the most as this has the longest synchronization time range. As the frequency deviation reaches synchronization faster, it can handle load variations at all the simulated times. The load change at 5 second results in almost the same phase angle deviation at the time of interconnection as in the reference scenario. The load change at 10 seconds also results in a phase deviation that is within the allowable limits after 25 seconds. However, both an increase and decrease in the load at 15 seconds result in phase deviations when the switch closes that are larger than the allowable limits

defined in this thesis.

The proposed synchronization technique can handle load decreases better than load increases. However, this is only valid when the load change occur early enough in the synchronization process. In the simulations where a load increase and decrease occur, Microgrid A has lower frequency than Microgrid B. As explained in Section 4, an increase in load results in a drop in the frequency of the system, while a decrease in load makes the frequency increase. Thus, in a synchronization process where the microgrid to be synchronized has lower frequency than the other, a decrease in load will help the synchronization process along since it will result in an increase in frequency. The synchronization process of the phase angle is much slower than that of the frequency. That means that if the load decrease comes after the frequency already is synchronized, then the load decrease does not have a positive effect as it will only make the frequency deviation shift away from its synchronized state.

8 Overall discussion

The purpose of this thesis is to suggest a synchronization control technique that enables a safe interconnection of two neighboring microgrids, without the risk of obtaining large inrush current transients. The proposed technique, which includes the elimination of deviations in frequency and phase angle through PI controllers, successfully synchronized the two grids. Thus, large inrush current transients were prevented when the two microgrids were interconnected.

The synchronization technique is required to make sure that the microgrids are able to change their operation from islanded to grid-connected mode at the interconnection moment. This entails that the microgrids in islanded operation, where set points of the frequency and voltage are internally decided, needs to change to follow common set points in the interconnected grid. This requirement is met by including synchronous generators in both microgrids, and designating the synchronous generator in one of the grids to complete the synchronization. The synchronous generators can be controlled to maintain the rated voltage and frequency of the grid. Thus, the converter-based units could continuously be operated in grid-following mode instead of having to change the operation from grid-forming to grid-following at the moment of interconnection. The synchronous generators in the two grids, due to their characteristics, will follow the same frequency when they operate in parallel in the common interconnected grid.

Microgrids generally have weak grid characteristics. When connecting a microgrid to a utility grid, a weak grid is connecting to a stiff grid. Thus, it is evident that the microgrid should synchronize its operation to that of the utility grid. However, when interconnecting microgrids to form multigrid configurations, multiple weak grids are to interconnect. Thus it is not evident which microgrid should act as a reference for the other, or if it is better that they both synchronize to a predefined reference point. In this thesis, it was chosen to synchronize one microgrid to follow the set point of the other. The microgrids used in the model were chosen to be of slightly different size. The smaller grid was chosen to synchronize to the larger one. This is less complex than to include both microgrids in the synchronization process. As both grids have weak characteristics, the grids might easily be subject to disturbances which has influence on the synchronization process.

In the model used for this thesis, only two microgrids were considered. The general idea with interconnected microgrids is that several microgrids in rural areas can form clusters

to increase the reliability. Several microgrids will then be present and it might not be apparent which microgrid should act as a reference for the synchronization. In addition, the number of microgrids that forms the multigrid might vary. It depends on the load demand across the neighboring microgrids, or if faults occur in one or several of the microgrids which will make them unavailable to connect with the multigrid configuration. Thus, it might be necessary to have several microgrids with the possibility of acting as reference for the others.

The microgrid, for which the synchronization technique was designed, was chosen to include a rotating machine in order to have an inertia component present. The presence of the inertia component makes the microgrid more reluctant to abrupt changes in its operating point. This adds a requirement to the synchronization process as it will require a larger time interval. With only converter-based units in the grid, the operating point of the grid could more swiftly change its operating point without risk of loosing stability.

The IEEE's GGOV1 gas turbine model was the choice of synchronous generator turbine model. However, this model is more generally used to model heavy-duty machines, whereas the synchronous generator intended for the microgrid model was much smaller. The model was adapted from a SINTEF model of a gas turbine synchronous generator. However, the base values were scaled down before the model was included in the multigrid model used in the simulations. There were some uncertainties related to whether this model would be the correct to use, or if the model would be insufficient to represent a synchronous generator of the wanted size. It was evaluated if it would be better to use a model of a microturbine. Microturbines are generally more used for the size range of interest in this project. However, microturbines have very high speed and is thus connected to low voltage distribution grids through voltage source converters. The purpose of having a synchronous generator component in the microgrids was to have an inertia component in the grid, and thus require the synchronization process to be conducted over a larger time period. Therefore, the idea of using microturbines was abandoned. Since the model of the synchronous generator received from SINTEF was designed in per unit values, it was assumed that the model would be accurate enough if all the base values of the system were correctly adjusted to smaller values. However, it might occur that smaller generators have slightly different values for the inertia constant and the reactances.

In the gas turbine model, used in the simulation model, the droop control of the synchronous generators is deactivated. Since there is only one synchronous generator present in each of the two microgrids, this is not critical. The droop control is meant to control the power sharing among the units. It will, however, be relevant for the interconnected operation of the microgrids. The simulations look at the synchronization process leading up to the point of interconnection, and a few moments after to see the effect of the synchronization. The simulations do not have any changes in generation or load after the switch closes. Thus, it is justifiable to not include the droop control for the simulations performed in this thesis. More exact simulations of interconnecting two microgrid, where variations in load may occur after the microgrids are connected, should include the droop control. Without droop control, load changes in the interconnected grid might cause poor power sharing among the units. Thus, some of the point with interconnected operation vanishes as a motivation for interconnecting microgrids is to achieve power support.

The proposed synchronization technique uses PI controllers for the phase angle and frequency deviations in a parallel configuration. The parallel configuration complicates the process of finding the PI controller gains. The synchronization loops proposed in this thesis were tuned through calculations for the frequency loop and through trial and error

for the phase angle loop. Since the synchronization technique is tuned partially through trial and error, optimal tuning for the loops may not have been found in this thesis. Other tuning techniques than what was tested might give better tuning results. Other configurations might also entail a better way to tune the PI controllers through calculations. Such a configuration could be a series configuration with the phase angle synchronization loop as an outer loop to the frequency synchronization loop. An attempt at this was performed in Section 5.3.2, but the tuning results did not synchronize the phase angles successfully. However, for the simulations performed in this thesis work, the PI gains found through trial and error give satisfactory results in synchronizing the phase angles.

The synchronization technique, with the found PI controller gains, was tested through simulations on a model consisting of two microgrids. The microgrids were defined to be of similar size. This was done to avoid that one of the microgrids would stand out as a strong grid in relation to the other. During the simulations it was assumed that the conditions in each grid were balanced. Thus, the synchronization technique was not tested for scenarios where the microgrids undergo unbalanced conditions. As remarked in Section 2, a challenge with microgrids is that unbalanced voltage conditions are becoming more prominent in microgrid operation. Thus, to look more closely at the synchronization process during occurrences of unbalanced condition might be of relevance for the topic of interconnecting microgrids. In addition, time delays in the communication link, transporting the synchronization control demands to the synchronous generator control, are not considered in this thesis work.

The simulations showed that the synchronization technique manage to eliminate the deviations in phase angle and frequency within the threshold values, and prevents the interconnection of the microgrids to result in high inrush current transients. This was also valid in scenarios were the conditions of the synchronizing grid were slightly altered. The general impression is that the synchronization loops manage to eliminate the deviations, although some grid conditions require longer time to reach synchronization. However, simulations will give better results than a real life system, as there are many assumptions related to the performed simulations, and only a restricted amount of operating conditions are tested in this thesis work.

The synchronization criteria set for this thesis is the thresholds values of 0.001 rad/s allowable phase deviation and 0.001 pu allowable frequency deviation. This translates to 0.06° phase angle deviation and 0.05 Hz frequency deviation. The chosen thresholds were adapted from the article [27]. The values might be stricter than needed to avoid damaging high inrush currents, especially for the phase angle deviation. For instance, the synchronization criteria determined in [29] included higher limit values. This criteria allows deviations of phase angles below 2° and frequency deviations below 0.1 Hz. The authors of [16] have chosen to follow the synchronization requirements from the IEEE 1547 standard, which allow deviations of 20% in phase angle deviations and 0.3 Hz in frequency deviations for microgrids of size smaller then 500 kVA.

The robustness of the synchronization loops was tested for different inertia constants of the synchronous machine. The different inertia constants had a significant effect on the effectiveness of the synchronization loops. The tuning was performed for the original inertia constant of the system. A simulation was conducted with inertia constant $H = 2$ seconds. From Figure 22 in Section 7.4, the deviations in frequency and phase angle oscillated much more for the lower inertia constant than in the reference scenario. Thus, the gains of the controller might be too large for the smaller inertia value. A few simulation tries with smaller gain values of the PI controllers in the synchronization loops were

conducted. From these simulation results, it can be concluded that it is possible to find an optimal tuning also for smaller inertia constants than in the reference scenario.

In a microgrid with multiple synchronous units, the system inertia is the weighted sum of the inertia of all the synchronous machines. It might not always be necessary to use all the synchronous generators in a microgrid to meet the load demand. Thus, the system inertia of the microgrid might vary with synchronous generators being turned on and off. As the system inertia will have an effect on the synchronization loops, they should be robust enough to cover synchronization for all operating conditions. Also for variable amount of synchronous generators that are activated during the synchronization.

9 Conclusion

The objective of this thesis work was to find a synchronization control technique that enables a seamless interconnection of two neighboring stand-alone microgrids, without the risk of high inrush current transients. The proposed synchronization strategy was tested out in a simulation model consisting of two simple microgrids. Several simulations were conducted with various adjustments to the microgrid conditions.

In the proposed synchronization technique, grid measurements from each of the two microgrids are used to calculate the phase angle and frequency deviations between the two grids. The deviation signals are passed through parallel PI controllers, one for the phase angle deviation and one for the frequency deviation. They are then added together and fed to the synchronous machine in the smallest microgrid as a speed reference offset. The chosen configuration of the synchronization loops cause the tuning process to be complicated. This resulted in the synchronization loops having to be partially tuned through trial and error. This is time consuming, and it might not result in optimal controller gains.

From the conducted simulations, the following could be observed:

1. The synchronization loops managed to eliminate the high inrush currents transients, giving a seamless interconnection of the two microgrids.
2. The synchronization loops diminished the deviations in frequency and phase angle within the chosen allowable limits.
3. With varying grid parameters, synchronization was generally achieved before the switch closed, 25 seconds into the simulation. Some of the variations would have required a longer synchronization period to produce the same level of synchronization as the reference scenario.
4. An important parameter that had great influence on the success of the synchronization technique was the inertia constant. Thus, this parameter value should be taken into account during the design process of the synchronization loops.

It can be concluded that a synchronization technique using the synchronous generator in one of the grids to synchronize the two microgrids shows promising results, and that the use of PI controllers to eliminate the deviations in phase angle and frequency is effective. However, more tests should be conducted on more detailed microgrid models and with more variations to the grid conditions.

10 Further work

The model description and the parameters used in this thesis work are included in the report to allow future research work to be based on this thesis. Throughout the thesis work, several challenges have arisen and been discussed. These challenges are summed up and listed below as proposals for future research.

1. Better procedures to tune the PI controllers in the synchronization loop.
2. Extend the model of the microgrid to become more detailed. Replace the current source at the DC side of the converter. Look at more intermittent power production and load demand that occur during a synchronization process.
3. Look at the performance of PI controllers to synchronize the grid under unbalanced conditions.
4. Include more than two microgrids in the multigrid configuration.

Bibliography

[1] S. A. Taher, M. Zolfaghari, C. Cho, M. Abedi and M. Shahidehpour, 'A new approach for soft synchronization of microgrid using robust control theory', *IEEE Transactions on Power Delivery*, vol. 32, no. 3, pp. 1370–1381, Jun. 2017.

[2] B. S. Hartono, Budiyanto and R. Setiabudy, 'Review of microgrid technology', in *2013 International Conference on Quality in Research, QiR*, 2013, pp. 127–132.

[3] L. K. Gan, D. E. Macpherson and J. K. Shek, 'Synchronisation control and operation of microgrids for rural/island applications', in *2013 48th International Universities' Power Engineering Conference (UPEC)*, 2013, pp. 1–6.

[4] D. T. Ton and M. A. Smith, 'The U.S. Department of Energy's Microgrid Initiative', *The Electricity Journal*, vol. 25, no. 8, pp. 84–94, Oct. 2012.

[5] R. H. Lasseter, 'Smart distribution: Coupled microgrids', in *Proceedings of the IEEE*, vol. 99, 2011, pp. 1074–1082.

[6] Y. Mekonnen and A. I. Sarwat, 'Renewable energy supported microgrid in rural electrification of Sub-Saharan Africa', in *2017 IEEE PES-IAS PowerAfrica*, 2017, pp. 595–599.

[7] C. X. Dou and B. Liu, 'Multi-agent based hierarchical hybrid control for smart microgrid', *IEEE Transactions on Smart Grid*, vol. 4, no. 2, pp. 771–778, 2013.

[8] Y. Li, J. Li, Y. Lei and W. Sun, 'Grid synchronization technology for distributed power generation system', in *2014 IEEE Conference and Expo Transportation Electrification Asia-Pacific (ITEC Asia-Pacific)*, Institute of Electrical and Electronics Engineers Inc., Oct. 2014, pp. 1–6.

[9] L. Fusheng, L. Ruisheng and Z. Fengquan, 'Chapter 5 - Protection of the microgrid', in *Microgrid Technology and Engineering Application*, Academic Press, 2016, pp. 69–89.

[10] A. Bidram and A. Davoudi, 'Hierarchical structure of microgrids control system', *IEEE Transactions on Smart Grid*, vol. 3, no. 4, pp. 1963–1976, 2012.

[11] Y. Yao and N. Ertugrul, 'An overview of hierarchical control strategies for microgrids', in *2019 29th Australasian Universities Power Engineering Conference (AUPEC)*, Nov. 2019.

[12] L. Meng, Q. Shafiee, G. F. Trecate, H. Karimi, D. Fulwani, X. Lu and J. M. Guerrero, 'Review on Control of DC Microgrids and Multiple Microgrid Clusters', *IEEE Journal of Emerging and Selected Topics in Power Electronics*, vol. 5, no. 3, pp. 928–948, Sep. 2017.

[13] A. Yazdani and R. Iravani, *VOLTAGE-SOURCED CONVERTERS IN POWER SYSTEMS Modeling, Control, and Applications*. John Wiley & Sons, Inc, 2010.

[14] S. Ansari, A. Chandel and M. Tariq, 'A Comprehensive Review on Power Converters Control and Control Strategies of AC/DC Microgrid', *IEEE Access*, vol. 9, pp. 17 998–18 015, Aug. 2021.

[15] U. B. Tayab, M. A. B. Roslan, L. J. Hwai and M. Kashif, 'A review of droop control techniques for microgrid', *Renewable and Sustainable Energy Reviews*, vol. 76, pp. 717–727, 2017.

[16] D. Shi, Y. Luo and R. K. Sharma, 'Active synchronization control for microgrid reconnection after islanding', in *IEEE PES Innovative Smart Grid Technologies Conference Europe*, 2014, pp. 1–6.

[17] M. Ghazavi Dozein, P. Mancarella, T. Kumar Saha and R. Yan, 'System Strength and Weak Grids: Fundamentals, Challenges, and Mitigation Strategies', in *2018 Australasian Universities Power Engineering Conference (AUPEC)*, 2018, pp. 1–7.

[18] National Grid ESO. (2020). 'What is Short Circuit Level?', [Online]. Available: https://www.nationalgrideso.com/news/what-short-circuit-level (visited on 30th Apr. 2021).

[19] D. Sun, X. Zhao, C. Lin, H. Pang, D. Shi, Z. Wang and C. Jing, 'Droop-based Control Scheme for MMC-HVDC Connected to Weak / Very Weak Grids', in *2019 IEEE Sustainable Power and Energy Conference (iSPEC)*, 2019, pp. 1947–1952.

[20] N. Mohan, T. M. Undeland and W. P. Robbins, *Power Electronics: Converters, Application and Design*, third. John Wiley and Sons, Inc, 2003.

[21] D. Holmes and T. Lipo, *Pulse Width Modulation for Power Converters: Principles and Practice*. John Wiley & Sons, Inc, 2003.

[22] C. Bajracharya, M. Molinas, J. A. Suul and T. M. Undeland, 'Understanding of Tuning Techniques of Converter Controllers for VSC-HVDC', in *Nordic Workshop on Power and Industrial Electronics*, Jun. 2008.

[23] D. P. Kothari and I. J. Nagrath, *Electric machines*, fifth. MC Graw Hill Education, 2018.

[24] P. Tielens, P. Henneaux and S. Cole, 'Penetration of renewables and reduction of synchronous inertia in the european power system – analysis and solutions', 2018.

[25] Task Force on turbine governor modeling, Power System Dynamic Performance and Power System Stability Subgroup, 'Dynamic Models for Turbine-Governors in Power System Studies', IEEE Power Energy Soc, Tech. Rep., 2013.

[26] NERC, 'Reliability Guideline - Application Guide for Modeling Turbine-Governor and Active Power-Frequency Controls in Interconnection-Wide Stability Studies', Tech. Rep., 2019.

[27] F. Giudicepietro, S. D'Arco, J. A. Suul and L. Piegari, 'Resynchronization of Islanded Virtual Synchronous Machines by Cascaded Phase and Frequency Controllers Acting on the Internal Power Reference', in *2020 9th International Conference on Renewable Energy Research and Application (ICRERA)*, Institute of Electrical and Electronics Engineers Inc., Sep. 2020, pp. 337–343.

[28] C. T. Lee, R. P. Jiang and P. T. Cheng, 'A grid synchronization method for droop controlled distributed energy resources converters', in *IEEE Energy Conversion Congress and Exposition*, 2011, pp. 743–749.

[29] C. Cho, J. H. Jeon, J. Y. Kim, S. Kwon, K. Park and S. Kim, 'Active synchronizing control of a microgrid', *IEEE Transactions on Power Electronics*, vol. 26, no. 12, pp. 3707–3719, 2011.

[30] N. S. Nise, *Control system engineering*, sixth. John Wiley and Sons, Inc, 2010.

[31] I. Wolfram Research, *Mathematica, Version 12.3*, Champaign, IL, 2021. [Online]. Available: https://www.wolfram.com/mathematica.

Appendix

A Synchronous generator circuit parameters

Parameters	Symbol	Value
Synchronous generator:		
Stator resistance	R_s	0.0027 pu
D-axis synchronous reactance	X_d	2.2 pu
D-axis transient reactance	$X_{d'}$	0.318 pu
D-axis subtransient reactance	$X_{d''}$	0.252 pu
Q-axis synchronous reactance.	X_q	1.25 pu
Q-axis subtransient reactance	$X_{q''}$	0.361 pu
Leakage reactance	X_l	0.15 pu
Inertia constant	H	2.96163 s
Friction factor	F	0
Number of poles	P	2
Excitation system:		
Time constant for LP filter of voltage measurement	T	0.05 s
Regulator input filter time constant	T_r	0.0001 s
Regulator output gain	K_a	400 pu
Regulator output time constant	T_a	0.02 s
Regulator denominator (lag) time constant	T_b	0 s
Regulator numerator (lead) time constant	T_c	0 s
Rate feedback excitation system stabilizer gain	K_f	0.03 pu
Rate feedback time constant	T_f	1 s
Maximum regulator output	$V_{a,max}$	14.5 pu
Minimum regulator output	$V_{a.min}$	-14.5 pu
Exciter field proportional constant	K_e	1 pu
Exciter field time constant	T_e	0.8 s
Rectifier loading factor proportional to commutating reactance	K_c	0.2 pu
Demagnetizing factor function of exciter alternator reactances	K_d	0.38 pu
Exciter output voltage for saturation factor SE(E1)	E1	4.18 pu
Exciter saturation factor at exciter output voltage E1	SeE1	0.1
Exciter output voltage for saturation factor SE(E2)	E2	3.14 pu
Exciter saturation factor at exciter output voltage E2	SeE2	0.03

B Simulink Model

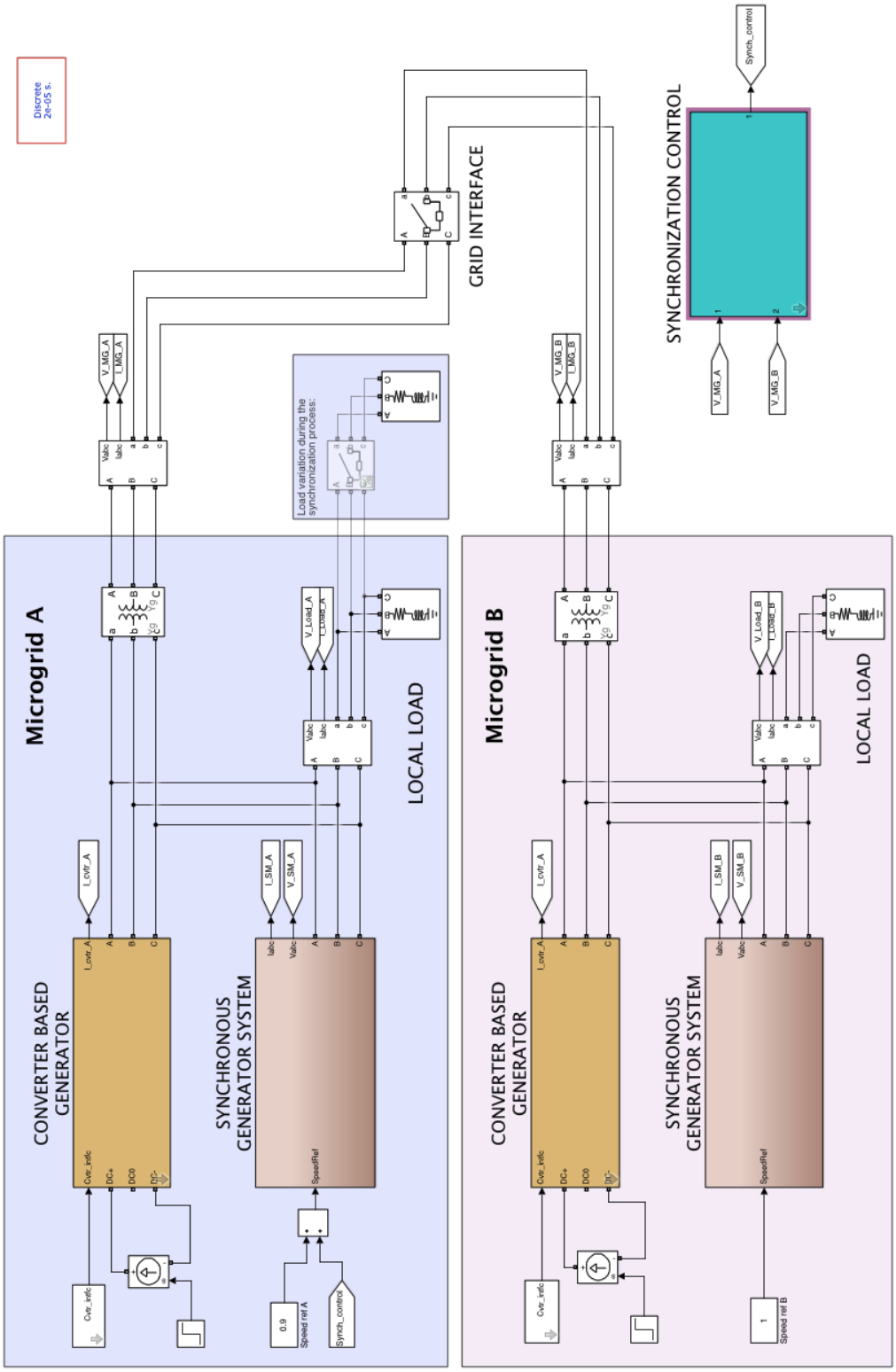

Figure 26: Simulink model: Overview of the multigrid topology.

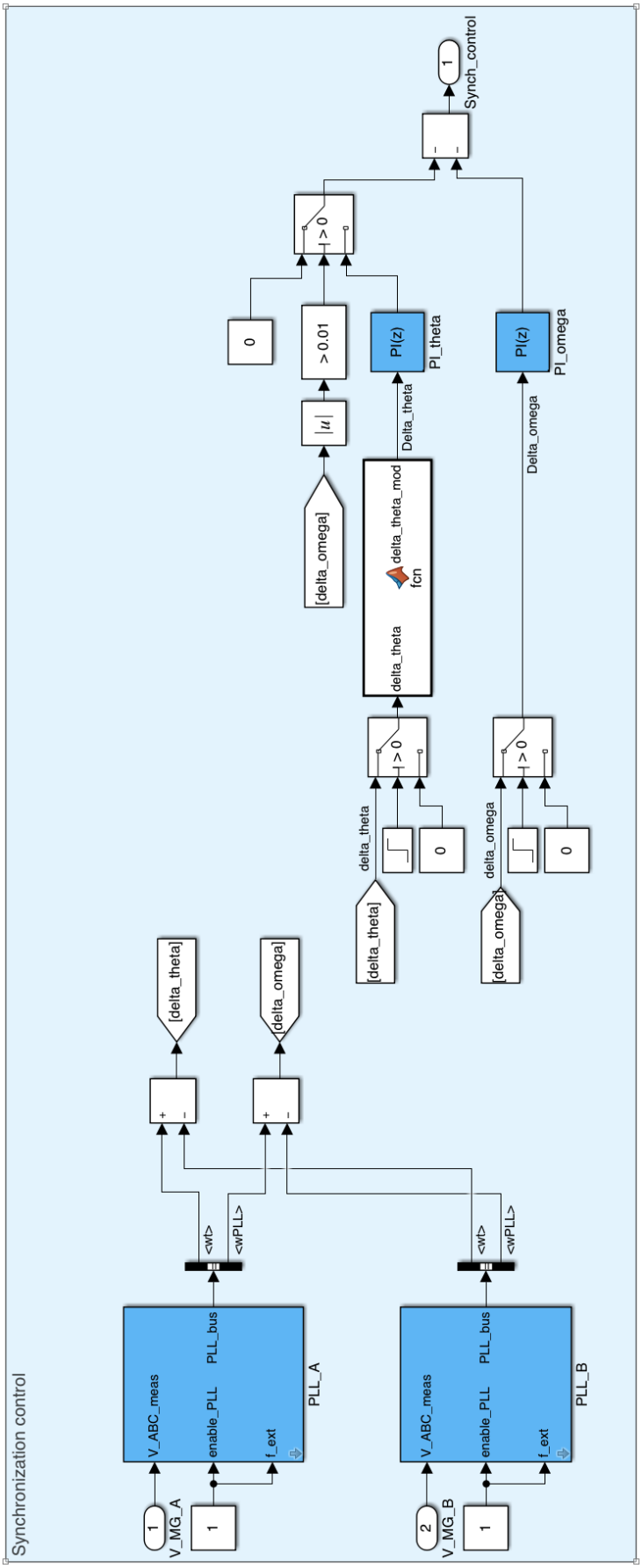

Figure 27: Simulink model: Synchronization control loops.

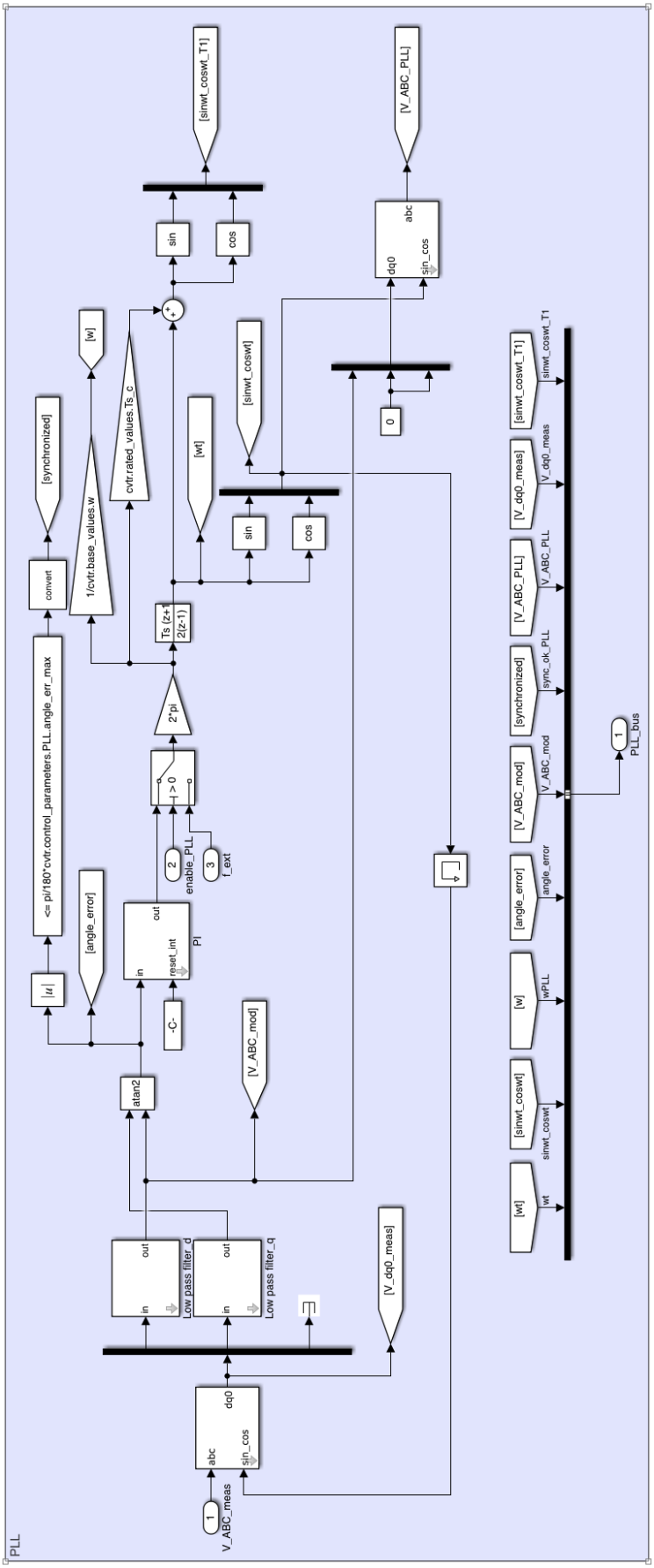

Figure 28: Simulink model: Phase Locked Loop (PLL).

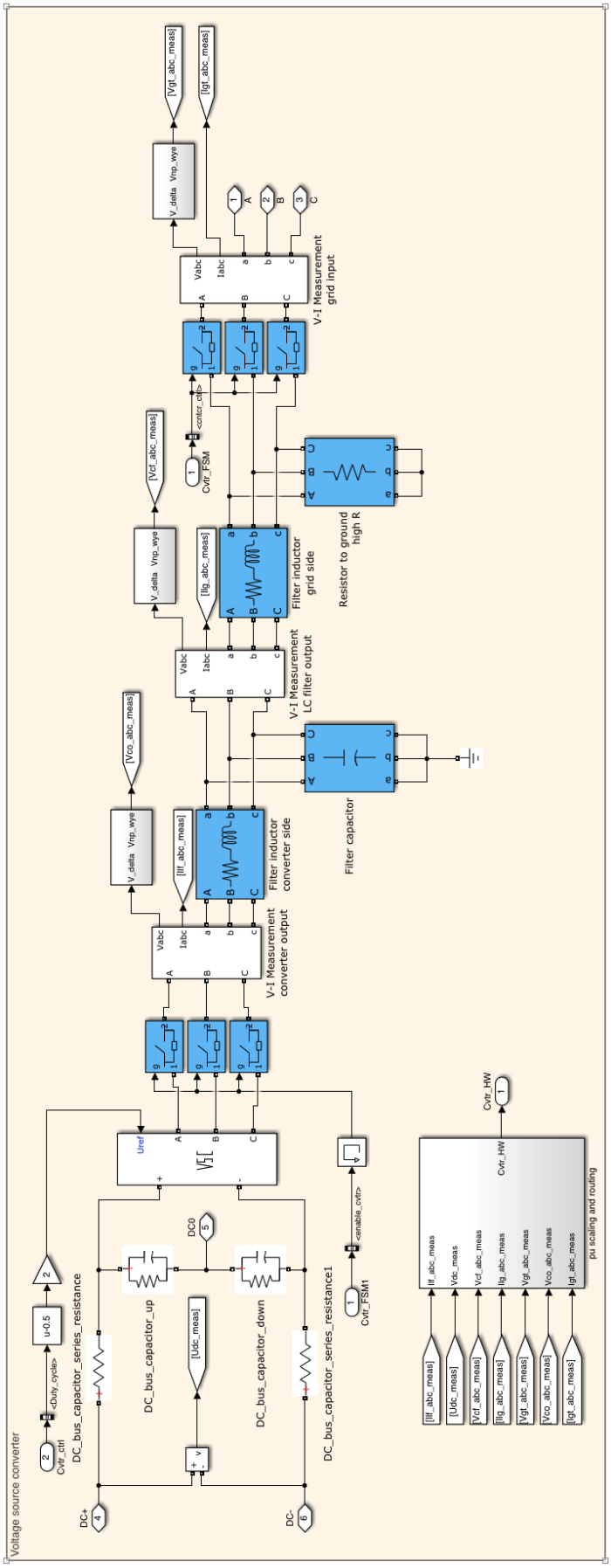

Figure 29: Simulink model: The 2-level average model voltage source converter.

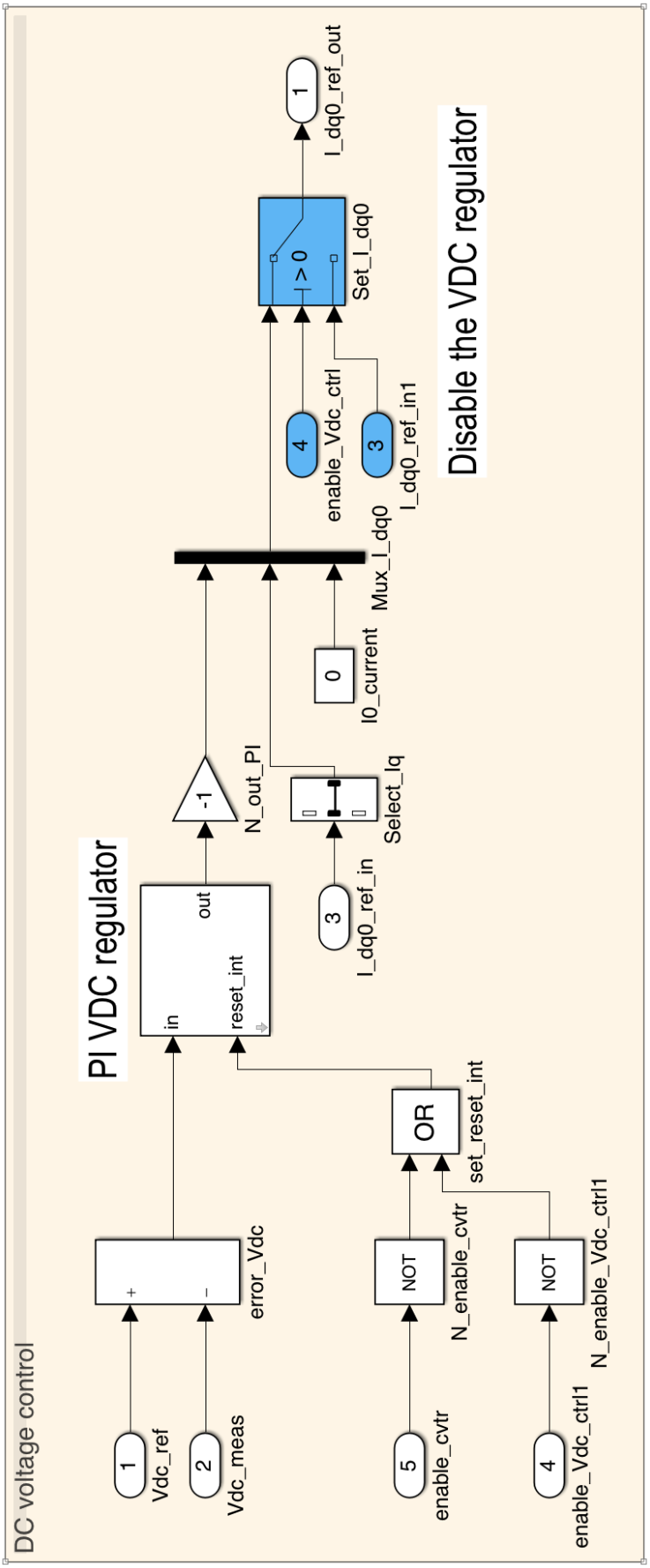

Figure 30: Simulink model: DC voltage control loop of the voltage source converter.

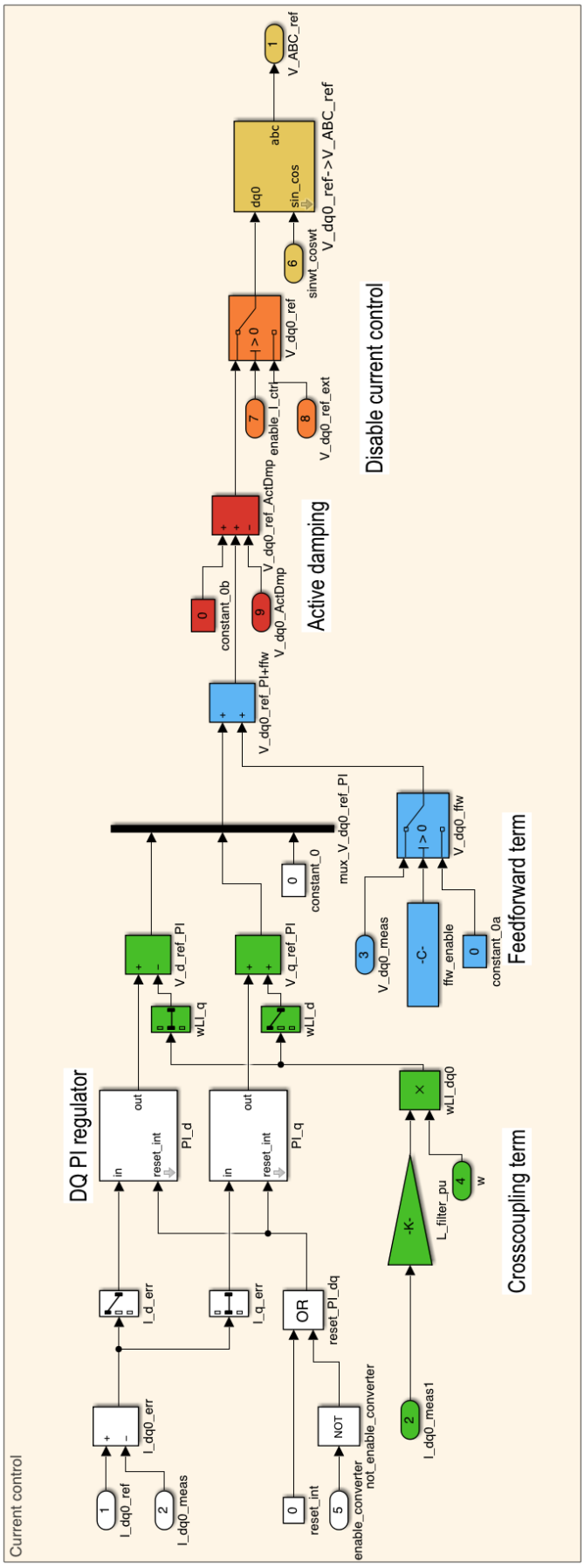

Figure 31: Simulink model: Current control loop of the voltage source converter.

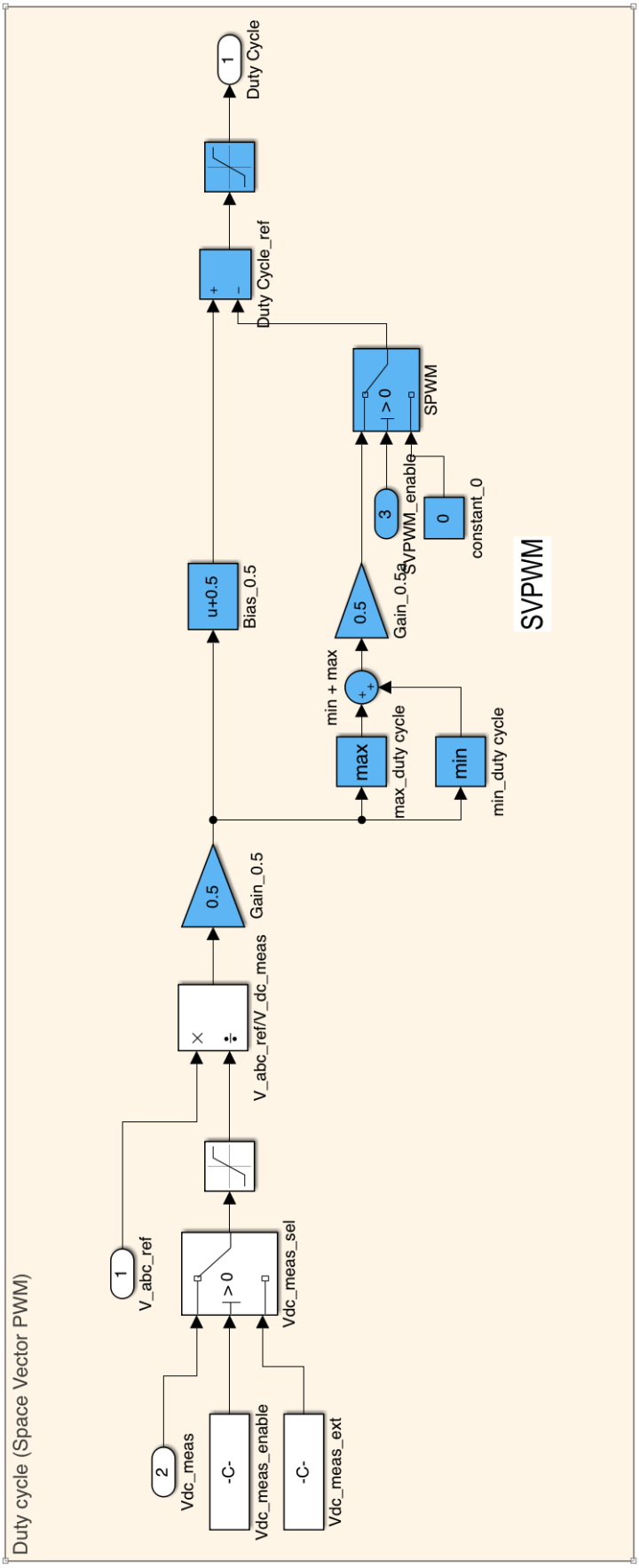

Figure 32: Simulink model: Space Vector Pulse Width Modulation (SVPWM) loop of the voltage source converter.

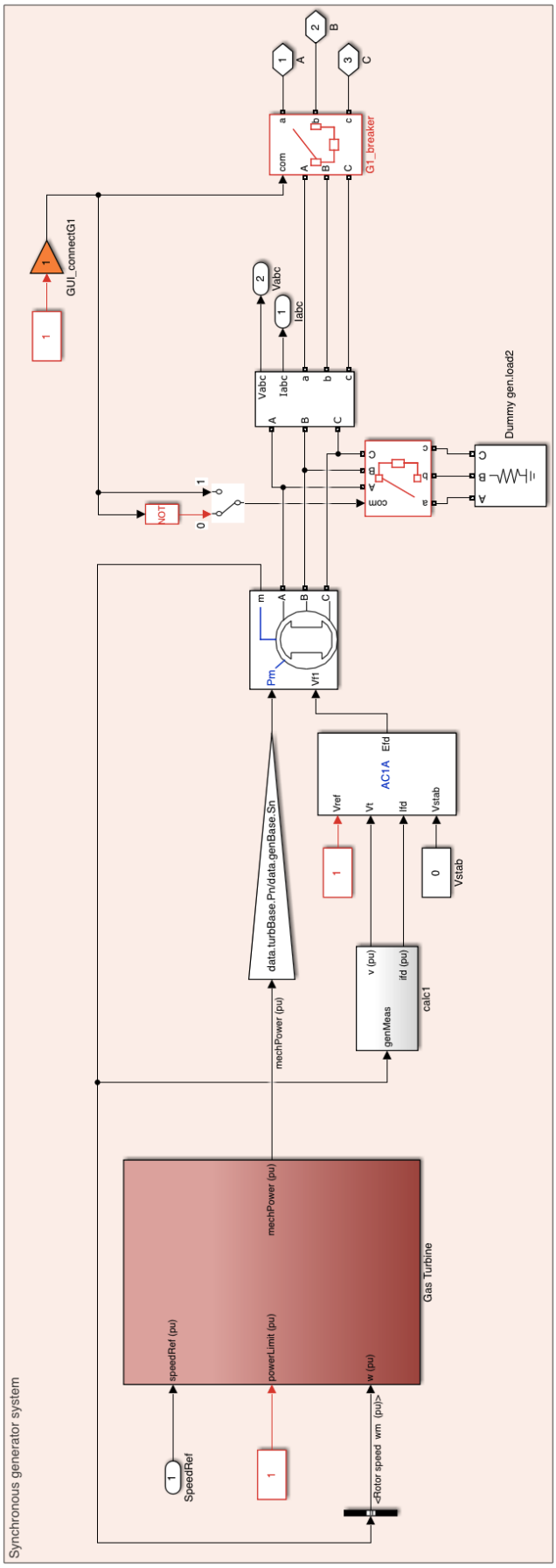

Figure 33: Simulink model: Synchronous generator system.

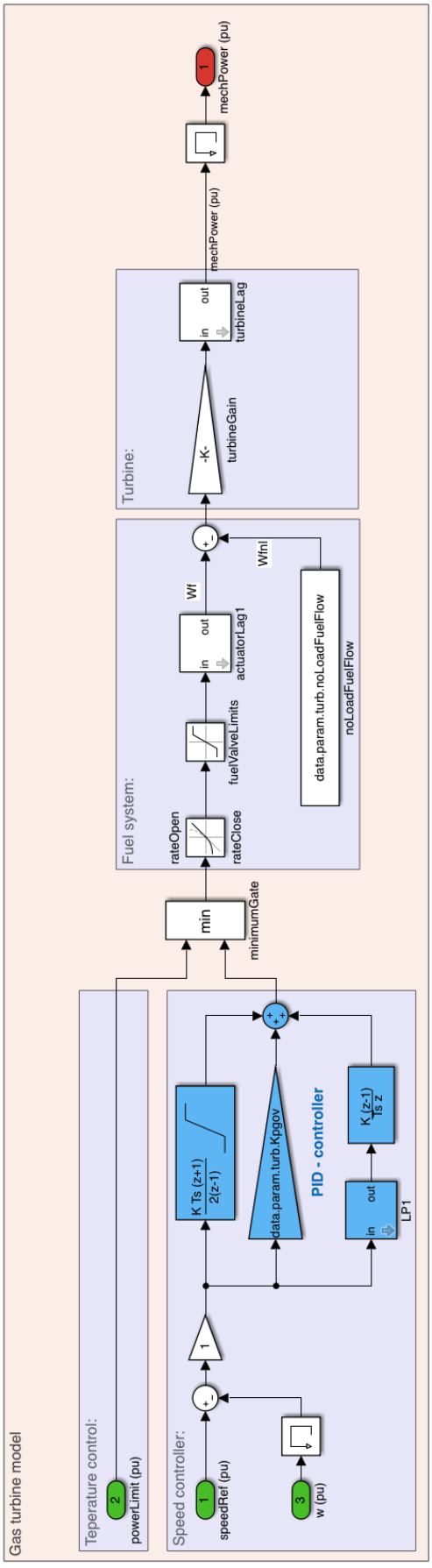

Figure 34: Simulink model: Gas turbine model of the synchronous generator system.

C Matlab scripts

```
%--------------------------------------------------------------------
% INITIALIZATION FILE FOR MULTIGRID SIMULINK MODEL
%--------------------------------------------------------------------

%% general simulation settings
Ts = 20E-6;          % simulation time step [s]
k_Ts = 1;            % ratio between simulation time step and
                     % control time step
Ts_c = k_Ts * Ts;    % control time step [s]

%% load settings for the converters
%%(e.g. ratings, protection settings)

Converter_settings;

%% load settings for the model for the electrical simulation

Electrical_components_settings;
%--------------------------------------------------------------------
```

```
%--------------------------------------------------------------------
% Converter_settings
%--------------------------------------------------------------------

converter_names = {'Converter_A'; 'Converter_B'; 'Converter_C'; ...
... 'Converter_D'};
converter_number = length(converter_names);

% Create a structure for each converter containing rated values,
% base values and circuit parameters.

cvtr.rated_values.Vn = 400;                          % Rms
cvtr.rated_values.In = 100e3/(sqrt(3)*400);
cvtr.rated_values.fn = 50;
cvtr.rated_values.Ts_c = 200e-6;
cvtr.rated_values.f_sw_ref = 5000;
cvtr.rated_values.Vdc_n = 700;

cvtr.circuit_parameters.R_filter_pu = .01;
cvtr.circuit_parameters.L_filter_pu = .1;
cvtr.circuit_parameters.C_filter_pu = .08;
cvtr.circuit_parameters.R_filter_AC_pu = .01;
cvtr.circuit_parameters.L_filter_AC_pu = .1;
cvtr.circuit_parameters.Cdc_pu = 4;
cvtr.circuit_parameters.Rdc_pu = 800;
cvtr.circuit_parameters.Rdc_series_pu = 2e-3;

%% Store the parameters into individual converter structures.

Converter_A = cvtr;
Converter_B = cvtr;
Converter_C = cvtr;
Converter_D = cvtr;

%% Calculates the base values
for i_cvtr = 1 : converter_number
  eval(strcat('cvtr = ',converter_names{i_cvtr}));
  cvtr = create_base_values(cvtr);
```

```
  cvtr.circuit_parameters.R_filter = ...
  ... cvtr.circuit_parameters.R_filter_pu * cvtr.base_values.Zac;
  cvtr.circuit_parameters.L_filter = ...
  ... cvtr.circuit_parameters.L_filter_pu * cvtr.base_values.Lac;
  cvtr.circuit_parameters.C_filter = ...
  ... cvtr.circuit_parameters.C_filter_pu * cvtr.base_values.Cac;

  cvtr.circuit_parameters.R_filter_AC = ...
  ... cvtr.circuit_parameters.R_filter_AC_pu * cvtr.base_values.Zac;
  cvtr.circuit_parameters.L_filter_AC = ...
  ... cvtr.circuit_parameters.L_filter_AC_pu * cvtr.base_values.Lac;

  cvtr.circuit_parameters.Cdc = ...
  ... cvtr.circuit_parameters.Cdc_pu * cvtr.base_values.Cac;
  cvtr.circuit_parameters.Rdc = ...
  ... cvtr.circuit_parameters.Rdc_pu * cvtr.base_values.Zdc;
  cvtr.circuit_parameters.Rdc_series = ...
  ... cvtr.circuit_parameters.Rdc_series_pu * cvtr.base_values.Zdc;

  eval(strcat(converter_names{i_cvtr},'= cvtr'));
end
% ------------------------------------------------------------------
```

```
% ------------------------------------------------------------------
% Create_base_values(cvtr) used in script Converter_settings
% ------------------------------------------------------------------

function [cvtr] = create_base_values(cvtr)

% Calculates the base values for the converter and saves the data
% in the converter structure in the substructure base_values

%% base for PU scaling
cvtr.base_values.Sac = cvtr.rated_values.Vn * cvtr.rated_values.In *sqrt(3);
    % [VA] base value for power ac side

cvtr.base_values.Vac = cvtr.rated_values.Vn * sqrt(2/3);
    % [V] base value for ac voltage (peak value of phase voltage)

cvtr.base_values.Iac = cvtr.rated_values.In * sqrt(2);
    % [A] base value for ac current (peak value of rated current)

cvtr.base_values.Zac = cvtr.base_values.Vac/cvtr.base_values.Iac;
    % [Ohm] base value for impedance

cvtr.base_values.f = cvtr.rated_values.fn;
    % [Hz] base value for grid frequency

cvtr.base_values.w = 2.*pi.*cvtr.base_values.f;
    % [rad/s] base value for angular frequency

cvtr.base_values.Lac = cvtr.base_values.Zac./cvtr.base_values.w;
    % [H] base value for inductance ac side

cvtr.base_values.Rac = cvtr.base_values.Zac;
    % [Ohm] base value for resistance ac side

cvtr.base_values.Cac = 1./(cvtr.base_values.w*cvtr.base_values.Zac);
    % [F] base value for capacitance ac side
```

```
cvtr.base_values.Sdc = cvtr.base_values.Sac;
    % [VA] base value for power dc side

cvtr.base_values.Vdc = 2*cvtr.base_values.Vac;
    % [V] base value for dc voltage

cvtr.base_values.Idc = cvtr.base_values.Sdc./(2.*cvtr.base_values.Vdc);
    % [A] base value for dc current

cvtr.base_values.Zdc = cvtr.base_values.Vdc/cvtr.base_values.Idc;
    % [Ohm] base value for impedance

end
%--------------------------------------------------------------------------
```

```
%--------------------------------------------------------------------------
% Parameter file for Multigrid Simulink model
%--------------------------------------------------------------------------
% Oda Skeie - Adapted from script by Olve Mo
% (Electrical_model_settings.m)
%--------------------------------------------------------------------------

%% System base values:

data.systemBase.Sn = 50e3; % VA
data.systemBase.Vn = 400;    % V rms line to line
data.systemBase.fn = 50; % Hz

%% Generator:

% Generator base values:
data.gen.Sn_pu = 1.0/0.8 ; % [pu] Generator rating in pu of system base
                           % Generator rating higher than system rating

data.genBase.Sn = data.gen.Sn_pu * data.systemBase.Sn  ; % VA
data.genBase.Vn = data.systemBase.Vn ;    % V rms phase to phase
data.genBase.fn = data.systemBase.fn;     % Hz

% Generator parameters:
data.param.gen.Rs = 0.00779/(11^2/42); % [pu] Stator resistance

data.param.gen.Xd = 2.2 ;        % [pu] D-axis synchronous reactance.
data.param.gen.Xd_ = 0.318;      % [pu] D-axis transient reactance
data.param.gen.Xd__ = 0.252;     % [pu] D-axis subtransient reactance
data.param.gen.Xq = 1.25 ;       % [pu] Q-axis synchronous reactance.
data.param.gen.Xq__ = 0.361;     % [pu] Q-axis subtransient reactance
data.param.gen.Xl = 0.15;        % [pu] Leakage reactance

data.param.gen.H = 2.96163;      % [s] Inertia constant
data.param.gen.F = 0;            % [?] Friction factor
data.param.gen.poles = 2;        % [-] Friction factor

% Creates vector for improved readability in mask:
data.param.gen.reactanceVectorSalient=[data.param.gen.Xd ...
... data.param.gen.Xd_ data.param.gen.Xd__ data.param.gen.Xq ...
... data.param.gen.Xq__  data.param.gen.Xl];

% Dummy generator load to get stable operation
data.param.gen.dummyP=0.1*data.genBase.Sn ;
    % Dummy generator load, connected whenever generator is
    % disconnected from grid(for numerical stability)
```

```
%% Automatic Voltage Regulator (same pu base as generator):
% - Tor Inge version

data.param.avr.T= 0.05 ;          % [s] Time constant for LP filter of voltage
                                  % measurement
data.param.avr.Tr= 0.0001 ;       % [s] Regulator input filter time constant
data.param.avr.Ka= 400 ;          % [pu] Regulator output gain
data.param.avr.Ta= 0.02 ;         % [s] Regulator output time constant
data.param.avr.Tb= 0 ;            % [s] Regulator denominator (lag) time
                                  % constant
data.param.avr.Tc= 0 ;            % [s] Regulator numerator (lead) time
                                  % constant
data.param.avr.Kf= 0.03 ;         % [pu] Rate feedback excitation system
                                  % stabilizer gain
data.param.avr.Tf= 1 ;            % [s] Rate feedback time constant
data.param.avr.Vamax= 14.5 ;      % [pu] Maximum regulator output
data.param.avr.Vamin= -14.5 ;     % [pu] Minimum regulator output
data.param.avr.Ke= 1 ;            % [pu] Exciter field proportional constant
data.param.avr.Te= 0.8 ;          % [s] Exciter field time constant
data.param.avr.Kc= 0.2 ;          % [pu] Rectifier loading factor proportional
                                  % to commutating reactance
data.param.avr.Kd= 0.38 ;         % [pu] Demagnetizing factor, function of
                                  % exciter alternator reactances
data.param.avr.E1= 4.18 ;         % [pu] Exciter output voltage for saturation
                                  % factor SE(E1)
data.param.avr.SeE1= 0.1 ;        % [-] Exciter saturation factor at exciter
                                  % output voltage E1
data.param.avr.E2= 3.14 ;         % [pu] Exciter output voltage for saturation
                                  % factor SE(E2)
data.param.avr.SeE2= 0.03 ;       % [-] Exciter saturation factor at exciter
                                  % output voltage E2

%% Gas turbine:

% Turbine base values:
data.turb.Pn_pu = 1.2 ; % [pu] Gas turbine rating in pu of system base
data.turbBase.Pn = data.turb.Pn_pu * data.systemBase.Sn  ; % W

% IEEE GGOV1 model
data.param.turb.turbinelagTb=0.1 ;      % [s] Turbine lag time constant
data.param.turb.turbineGainKturb=1.873 ;% [-] Turbine gain
data.param.turb.noLoadFuelFlow=0.17 ;   % [pu] No load fuel flow
data.param.turb.actuatorTact = 0.2 ;    % [s] Fuel flow actuator time
                                        % constant
data.param.turb.vMax = 0.704 ;          % [pu] Maximum fuel valve opening
data.param.turb.vMin = 0.09 ;           % [pu] Minimum fuel valve opening
data.param.turb.rateOpen = 3.3 ;        % [pu/s] Maximum rate of increase
                                        % fuel command
data.param.turb.rateClose = -3.3 ;      % [pu/s] Maximum rate of decrease
                                        % fuel command

data.param.turb.Kpgov= 5.5 ;    % [-] Governour proportional gain
data.param.turb.Kigov=  2 ;     % [-] Governour integral gain
data.param.turb.Tdgov= 1 ;      % [s] Time constant for derivative gain

data.param.turb.droopT = 0.02 ; % [s] Time constant for electric power
                                % transducer

%% Trafo1:

data.param.trafo1.pn = 200e3;   % VA
```

```
data.param.trafo1.fn = 50;        % Hz
data.param.trafo1.V1n = 20e3;     % V
data.param.trafo1.r1_pu = .01;    % [pu]
data.param.trafo1.l1_pu = .04;    % [pu]
data.param.trafo1.V2n = 400;      % V
data.param.trafo1.r2_pu = .01;    % [pu]
data.param.trafo1.l2_pu = .04;    % [pu]

% Creates vector for improved readability in mask
data.param.trafo1.winding1 = [data.param.trafo1.V1n ...
... data.param.trafo1.r1_pu data.param.trafo1.l1_pu];
data.param.trafo1.winding2 = [data.param.trafo1.V2n ...
... data.param.trafo1.r2_pu data.param.trafo1.l2_pu];

% ------------------------------------------------------------------
```

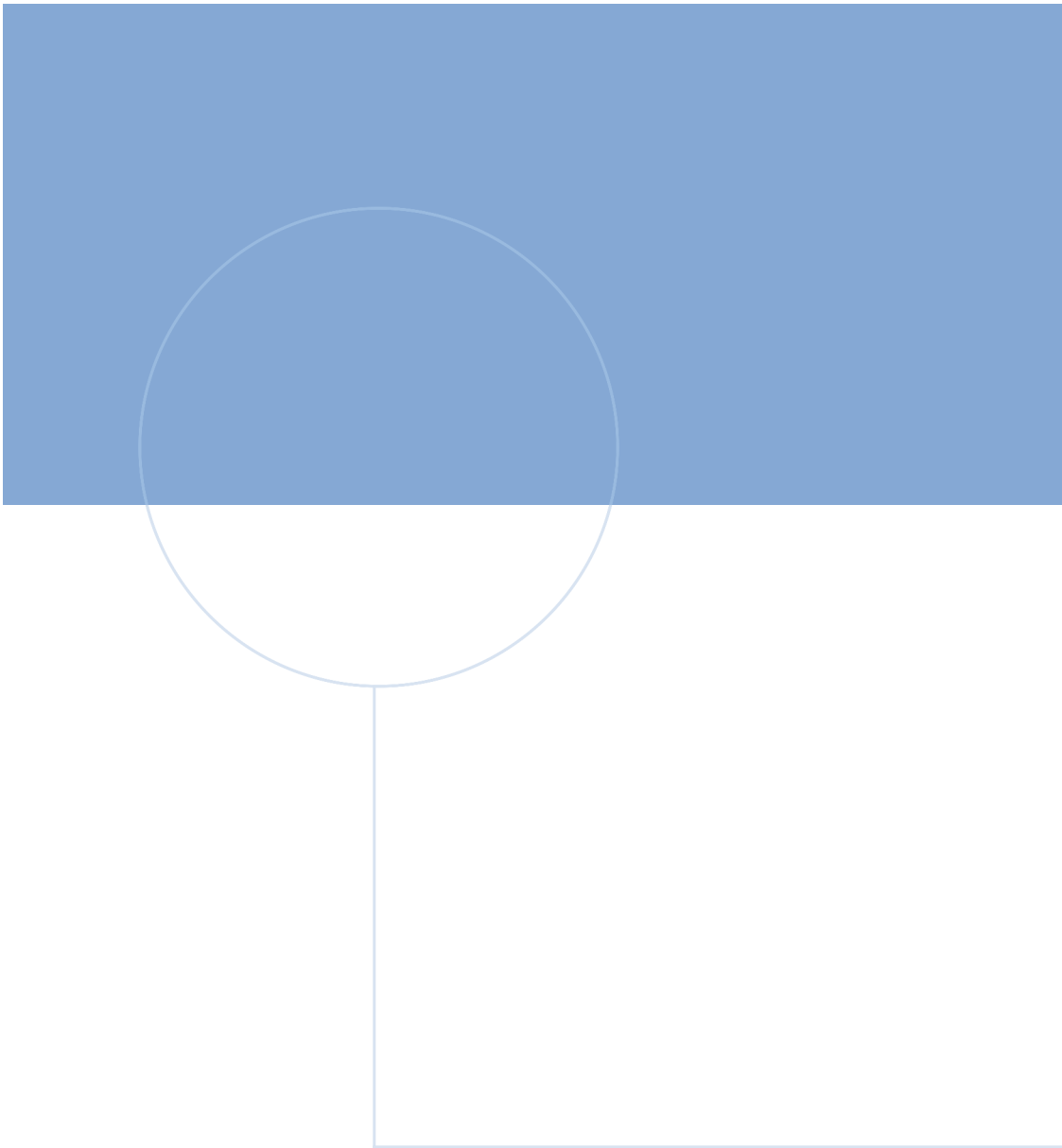

NTNU

Kunnskap for en bedre verden